EIR-Bericht Nr. 217

EIR-Bericht Nr. 217
NEANDC (OR) - 143 "U"
INDC (SWT) - 009 / L

Eidg. Institut für Reaktorforschung Würenlingen
Schweiz

Neutron Capture Cross Section Measurements in the Energy Region from 0.01 to 10 Electron Volts

F. Widder

Würenlingen, April 1975

EIR - Report No. 217
NEANDC (OR) - 143 "U"
INDC (SWT) - 009/L

Neutron Capture Cross Section Measurements in the Energy Region from 0.01 to 10 Electron Volts

F. Widder

April 1975

ABSTRACT

Absolute neutron capture cross section measurements from 0.01 to 10 eV using a Moxon-Rae detector are described. For the calculation of multiple scattering and gamma attenuation effects in samples new improved methods were developed. Cross section curves were evaluated for the elements Vanadium, Manganese, Cesium, Europium, Dysprosium, Lutetium and Tantalum as well as for the isotopes ^{151}Eu, ^{153}Eu, ^{175}Lu and ^{176}Lu. The accuracy attained is 2-4 % from 0.01 to 1 eV and 3-5 % above 1 eV. For some resonance cross sections above 4 eV the total error increases up to 10 %.

CONTENTS

I. INTRODUCTION

Neutron capture cross sections in the thermal and epithermal energy region are still required for several elements and isotopes. These cross sections are needed for different purposes such as detector applications, fission product poison calculations, burn-up calculations, flux measurements and others.

In order to fulfil requests for neutron data the capture cross sections for the elements Vanadium, Manganese, Cesium, Europium, Dysprosium, Lutetium and Tantalum have been measured in the neutron energy range from 0.01 through 10 eV. The cross sections of the isotopes ^{151}Eu, ^{153}Eu, ^{175}Lu and ^{176}Lu were determined by means of additional measurements on samples enriched in ^{153}Eu and ^{175}Lu, respectively.

A special interest was taken in the Dysprosium- and Lutetium cross sections. Dysprosium has found a widespread application as an activation detector for thermal neutron fluxes as its cross section obeys nearly the 1/v-law and the resonance integral is relatively small. It is also suited as burnable poison material. Lutetium is a convenient detector for the determination of the neutron temperature because, on account of the resonance at 0.14 eV in ^{176}Lu, the activation of a given lutetium foil becomes strongly temperature dependent.

The Manganese cross section is needed for precise standardization of emission rates of neutron sources and the Cesium- and Europium cross sections are useful for fission product poison calculations.

Besides the well known capture cross sections of Gold and Indium the Tantalum cross section is considered to be useful

as a standard for neutron capture cross section measurements. Up to the present the values of this cross section between 0.01 and 10 eV were determined only with poor accuracy.

The requests for the above mentioned cross sections are characterized by - from the experimental point of view - high accuracy requirements. For this reason we had to develop new improved methods for the determination of background and dead time corrections as well as for the calculation of multiple neutron scattering and gamma-ray attenuation effects in samples in order to reduce the systematic errors.

II. FACILITY

The neutron source used in these measurements was the thermal reactor DIORIT (24 MWth) of the Swiss Federal Institute for Reactor Research (EIR). The neutron spectrum coming out from the collimator of the radial beam tube shows a Maxwellian distribution for energies less than 0.25 eV and an 1/E-behaviour for higher energies. After having passed through a parallel plate type fission counter which served as flux monitor, the neutron beam was pulsed by means of a fast chopper.

The chopper rotor consists of a K-Monel (66 % Ni, 29 % Cu, 3 % Al, 1 % Fe, 1 % Mn) disk of 210 mm diameter with a slit package of six straight slits, each 1.4 mm in width. The rotating speed can be adjusted between 1500 and 24000 rpm and kept constant within ± 0.5 %. Two slit collimators,

one in front of, the other behind the chopper are used to produce a relatively narrow spot size at the sample, located 15 m from the rotor, as well as to reduce the background due to fast neutrons and gamma-rays from the centre of the reactor.

The neutron energy was determined by conventional time-of-flight techniques. The effective flight-path length was 15.34 metres. The entire flight path was maintained at a pressure of less than 10^{-3} mm Hg, including an additional 0.4 m beyond the sample. The timing pulses (start pulses) for the multichannel time-of-flight analyzer were produced by the chopper itself in the following way: A collimated beam between a light-source and a photomultiplier is interrupted by the rotating disk. Each time the rotor slits are parallel to the incident neutron beam, this channel is opened by a built-in diaphragm which is provided with a rectangular slit. Thus, a triangular pulse is generated whose maximum corresponds to the moment of maximum neutron transmission. The start-pulses are obtained from the differentiated triangular pulses by means of a timing discriminator, the output signals of which are accurately timed to the crossover point of the bipolar input pulses.

As multichannel time analyzer the LABEN-Correlatron-1024 system in connection with the time-of-flight unit TV 60/4096 was used. The main features of this system are:

- adjustable channel groups : 1024, 512, 256, 128.
- channel width variable in steps of factor 2 from 0.125 to 128 µsec.
- built-in delay of the start-pulse variable in steps equal to 2^4, 2^5, 2^6,....., 2^{19} µsec multiplied by a number between 1 and 9. A delay ranging from 0 to 4'718'592 µsec

can thus be introduced.

- fixed dead time : 8 μsec for any channel width.

For the measurement of pulse-height spectra the TOF-unit was replaced by a fast converter, type LABEN FC 60/4096.

The whole electronic equipment of the TOF-spectrometer, inclusive control units and alarm circuits, as well as the mechanical setup are described in detail elsewhere (1),(2).

III. DETECTOR

The capture cross sections reported in this paper were measured by observing the prompt gamma-rays that are emitted by the compound nucleus upon neutron capture. In general, several gamma-rays are emitted whose spectral distribution is a function of the capturing isotope and the neutron energy. The total energy of the gamma-rays ($E_{\gamma,tot}$) is very nearly equal to the neutron binding energy (E_B) of the compound nucleus. The difference between the prompt gamma-ray energy and the neutron binding energy is due to the kinetic energy of the neutron being captured, which is very small at the neutron energies considered here and can be neglected. Since it is usually not possible to make corrections for changes in gamma spectra with neutron energy, the gamma-ray detector should have a detection efficiency that is independent of the gamma spectrum. This has been achieved by the Moxon-Rae detector (MRD) that was used for these measurements. Its efficiency shows a good linearity with gamma-ray energy and amounts to about 0.25 percent per MeV. This property implies that the efficiency

for detecting a capture event is proportional to the total gamma-ray energy i.e. to the neutron binding energy of the compound nucleus being studied.

Details of the detector construction are given in (3). Briefly, the detector consists of four plastic scintillators (NE 102 A, diameter 10 cm, thickness 0.05 cm) mounted on four photomultipliers (EMI 9530 B) symmetrically surrounding an evacuated aluminum tube (diameter 9 cm), which contains the sample. Between the scintillator disks and the aluminum tube there are slabs of graphite (thickness 3 cm) forming a cube of 15 x 15 x 15 cm. The graphite (density 1.70 g/cm^3) serves as gamma-ray to electron converter. The scintillator sheets, by means of which the electrons are detected, are coated with a thin aluminum reflector, which was deposited by vacuum evaporation. A typical pulse height spectrum as well as the discriminator setting are shown in Figure 1.

IV. DETECTOR CALIBRATION

The efficiency of the detector was determined by means of calibrated gamma-ray sources up to 4 MeV total gamma-energy and by the saturated resonance technique between 6 and 9 MeV. The most important properties of the gamma-sources used are listed in Table I. The absolute activities during the calibration measurements were about 10 µCi, the accuracies are given in column 4. The gamma-ray self-absorption effect of the sources was ≤ 0.2 %, hence, no correction was necessary. Thus, the detector efficiency is given by

$$\varepsilon_{MRD} = \frac{C}{A \cdot t} \qquad (4.1)$$

where

C = counts observed, corrected for background and dead time

A = activity of the gamma-source (dps)

t = counting time (sec) .

TABLE I

Gamma-sources used for calibration

nuclide	$E_{\gamma,tot}$	$T_{1/2}$	$\Delta A/A$
Cs 137	0.662 MeV	30.6 y	± 1.1 %
Mn 84	0.835	312.7 d	0.5
Fe 59	1.185	45.0 d	1.0
Na 22	2.196	2.602 y	0.8
Co 60	2.506	5.264 y	0.5
Y 88	2.646	107.4 d	1.0
Na 24	4.122	15.00 h	1.0

The neutron resonances used for calibration above 5 MeV are listed in Table II. The saturated resonance technique consists in measuring the counting rate of prompt γ-rays from

TABLE II

Neutron resonances used for calibration

nuclide	$E_{n,res}$	$E_B = E_{\gamma,tot}$
Ta 181	4.28 eV	6.063 MeV
Rh 103	1.26	6.999
Sm 149	0.098	7.985
Cd 113	0.178	9.041

a sample which captures essentially all of the incident

neutrons in the resonance region. This is indicated by a flattened resonance peak in the time-of-flight spectrum. It is important that capture predominates over scattering in order to reduce the corrections for scattered neutrons, and the thickness of the sample material must not be sufficient to produce considerable gamma absorption effects. The detector efficiency is then obtained from

$$\varepsilon_{MRD} = \frac{C}{C_m \cdot \Phi_n \cdot F_s} \cdot \frac{\sigma_t/\sigma_c}{1-T_n} \cdot \frac{1}{f_{sc}} \cdot \frac{1}{f_{ab}} \qquad (4.2)$$

where

C = counts observed, corrected for background and dead time

C_m = monitor counts observed during the measurement

Φ_n = number of incident neutrons per monitor count and cm^2

F_s = sample area (cm^2)

T_n = transmission of incident neutrons through the sample

σ_c = Doppler-broadened capture cross section of the sample material

σ_t = Doppler-broadened total cross section of the sample material

f_{sc} = correction factor due to multiple neutron scattering in the sample

f_{ab} = correction factor due to gamma-ray self-absorption in the sample.

The determination of the number of incident neutrons or the absolute neutron flux, respectively, is described in the next section of this paper. The methods used for the calculation of multiple scattering effects as well as of gamma-ray self-absorption effects will be treated subsequently. In its final form the relationship (4.2) becomes

$$\varepsilon_{MRD} = \frac{C}{C_m \cdot \Phi_n \cdot F_s} \cdot \frac{1+\frac{\sigma_s}{\sigma_c} \cdot TQ}{1-T_n} \cdot \frac{1}{S_\gamma} \qquad (4.3)$$

where

σ_s = scattering cross section (total minus capture) of the sample material

TQ = average transmission of scattered neutrons.

Since $TQ < T_n << 1$ and $\sigma_s/\sigma_c << 1$ for the resonances considered here, only rough cross section values are needed for the calculation of the scattering correction factor. The self-absorption factor S_γ ($\leqslant 1$) represents the mean gamma-ray transmission averaged over the whole capture gamma-ray spectrum.

The results of the calibration measurements are shown in Figure 2. By means of a least-squares fit the following value for the detector efficiency per MeV was found:

$$\frac{\varepsilon_{MRD}}{E_{\gamma,tot}} = \varepsilon_o = 0.253 \pm 0.003 \ \% \ / \ MeV \qquad (4.4)$$

V. FLUX MEASUREMENT

Once the detector efficiency per MeV has been determined the incident neutron flux can be measured by means of a sample material whose capture cross section is already well known and much greater than the scattering cross section. These conditions are fulfilled very well by the gold cross section. However, due to the resonance at 4.91 eV this standard is not suitable in the energy range between 2 and 10 eV because the accuracy of the flux determination decreases with increasing gradient of the standard cross section.

Another possibility consists in the application of the $^{10}B(n,\alpha\gamma)^{7}Li$-reaction whose cross section is proportional to the inverse of the neutron velocity (1/v - law) over the whole region of interest. Unfortunately the gamma-ray energy is only 0.478 MeV, thus lying far below the region of neutron binding energies. Furthermore, the linearity of detector efficiency with gamma-energy becomes worse for energies below 0.5 MeV and, hence, the accuracy decreases too.

For these reasons we have applied a new method for the determination of the absolute neutron flux at the sample : A ^{6}Li-loaded glass scintillator (NE 912) of the same diameter (1½") was mounted on a two inch photomultiplier (EMI 6097S). A thick (10 mm) diaphragm of sintered B_4C (density 2.49 g/cm^3) was fixed in front of the scintillator in order to avoid background counts due to neutrons which are scattered by the surrounding materials (multiplier, housing, etc.). The whole assembly was placed inside the evacuated through tube so that the scintillator was located in the same position as the capture samples before. The construction of this assembly as well as of the sample-holder used for the capture cross section measurements, allowed a quick exchange of the two from the end of the tube. Before each exchange the flight tube had to be filled with air and afterwards evacuated again. In order to get a short evacuation time the flight tube was provided with a pipeline valve just before the shielding of the MRD, thus only a small part of the whole flight tube had to be filled and re-evacuated.

The glass scintillator used consists of (composition by weight) 17.0 % $^{6}Li_2O$, 0.9 % $^{7}Li_2O$, 2.6 % Ce_2O_3 and 79.5 % SiO_2 . The total macroscopic cross section of this

material can be written

$$\Sigma_t = a_1 + \frac{a_2}{\sqrt{E_n}}$$

a_1 and a_2 being constants. The first term is due to scattering, the second one due to the $^6Li(n,\alpha)^3T$ - reaction. All other reactions, e.g. (n,γ), are negligible. In order to get exact values for a_1 and a_2 separate measurements were carried out using the scintillator-disk as a neutron filter and a second scintillator of the same kind as neutron detector. Thus, the neutron transmission (T_{no}) of the scintillator could be determined over the entire energy range from 0.01 to 10 eV.

Using the equations

$$T_{no} = \exp(-\Sigma_t d_o)$$

$$\ln \frac{1}{T_{no}} = \Sigma_t d_o = c_1 + \frac{c_2}{\sqrt{E_n}} \qquad (5.1)$$

$$(c_1 = a_1 d_o \ , \quad c_2 = a_2 d_o) \ ,$$

d_o being the thickness of the scintillator, the parameters c_1 and c_2 were found by means of a least-squares fit :

$$\begin{aligned} c_1 &= 0.02169 \pm 0.00197 \\ c_2 &= 0.25025 \pm 0.00080 \quad (eV^{1/2}) \\ \text{for } d_o &= 0.10 \text{ cm} . \end{aligned} \qquad (5.2)$$

This shows that the ^6Li-glass-scintillator (LID) is a suitable flux detector up to 100 eV because the (n,α)-reaction predominates over scattering, the neutron

capture is essentially radiationless and the response curve (Figure 3) affords excellent pulse height discrimination against background gamma radiation. Furthermore the intrinsic efficiency of the detector is very close to 100 % because of the small ranges of the α- and T-particles within the scintillator materials.

The absolute neutron flux Φ_n per channel is thus given by

$$\Phi_n = \frac{N_o}{C_{mo} \cdot F_o} \cdot \frac{\Sigma_\alpha + \Sigma_s}{\Sigma_\alpha} \cdot \frac{1}{1-T_{no}} \cdot \frac{1}{f_{so}}$$

With $f_{so} = \dfrac{1+\Sigma_s/\Sigma_\alpha}{1+\Sigma_s \cdot TQ_o/\Sigma_\alpha}$ it follows that

$$\Phi_n = \frac{N_o}{C_{mo} \cdot F_o} \cdot \frac{1+\Sigma_s \cdot TQ_o/\Sigma_\alpha}{1-T_{no}} \qquad (5.3)$$

Using the parameters c_1 and c_2 the relationship (5.3) can be written

$$\Phi_n = \frac{N_o}{C_{mo} \cdot F_o} \cdot \frac{1+c_1 \cdot TQ_o \cdot \sqrt{E_n}/c_2}{1-\exp(-c_1-c_2/\sqrt{E_n})} \qquad (5.4)$$

where

Φ_n = number of incident neutrons per monitor count and cm^2

N_o = counts observed, corrected for background and dead time

F_o = scintillator area (cm^2)

C_{mo} = monitor counts observed during the measurement

Σ_s = macroscopic scattering cross section

Σ_α = macroscopic (n,α)-cross section

f_{so} = correction factor due to multiple scattering of neutrons within the scintillator

E_n = neutron energy (eV)

T_{no} = neutron transmission of the scintillator

TQ_o = $TQ(T_{no}, d_o, r_o)$ = average transmission of scattered neutrons (r_o = scintillator radius).

VI. CROSS SECTION MEASUREMENTS

The capture cross sections reported in this paper were measured by means of samples of various thicknesses using various chopper speeds, neutron burst widths, time channel widths and delays of start pulses. These parameters were optimized with respect to energy resolution and systematic as well as statistical errors in order to get data of sufficient accuracy in a reasonable time. For each measurement three time-of-flight spectra had to be determined:

RUN 1 : Spectrum of capture detector (MRD), sample in

RUN 2 : Spectrum of flux detector (LID), sample out

RUN 3 : Spectrum of flux detector, sample in filter position just behind the chopper

The shapes of the time-dependent backgrounds were determined by repeating the three runs with an additional boron-carbide filter which absorbed essentially all thermal and low epithermal neutrons ($T = 0.003$ for $E_n = 10$ eV). These background spectra were corrected for the fast neutron transmission of the B_4C-filter (details are described in section VIII) and then normalized to the exact background rates in the following way : The channel width, the total

number of channels and the delay of the timing pulses were chosen so that the last 50 channels of the time-of-flight spectra mentioned above corresponded to neutron energies lying below the chopper cut-off energy. Thus, the accumulated counts in those channels indicated the upper tail of the exact background curve, and the absolute normalization factor could be found by comparison with the separately measured background spectra.

VII. CROSS SECTION ANALYSIS

The counting rate observed in a time channel of RUN 1, corrected for background and dead time, can be written

$$\frac{N_c}{C_{mc}} = \Phi_n \cdot F_s \cdot \varepsilon_{MRD} \cdot \frac{\sigma_c}{\sigma_t} \cdot (1-T_n) \cdot f_{sc} \cdot f_{ab} \qquad (7.1)$$

where F_s is the sample area and Φ_n is given by equation (5.4) which contains N_o, the counts observed in RUN 2. The neutron transmission of the sample T_n is determined by the number of counts N_t observed in RUN 3 :

$$T_n = \frac{N_t}{N_o} \cdot \frac{C_{mo}}{C_{mt}} \qquad (7.2)$$

C_{mo}, C_{mt} being the corresponding monitor counts. Using the relation

$$f_{sc} = \frac{1+\frac{\sigma_s}{\sigma_c}}{1+\frac{\sigma_s}{\sigma_c}\cdot TQ} = \frac{1}{TQ+\frac{\sigma_c}{\sigma_t}(1-TQ)} \qquad (7.3)$$

for the multiple scattering correction factor and solving equation (7.1) for the capture cross section σ_c, we obtain

$$\sigma_c = \frac{p \cdot \sigma_t \cdot TQ}{1 - p \cdot (1 - TQ)} \tag{7.4}$$

with $$p = \frac{N_c}{C_{mc} \cdot \Phi_n \cdot F_s \cdot (1 - T_n) \cdot \varepsilon_{MRD} \cdot S_\gamma} \tag{7.5}$$

and $$\sigma_t = \frac{1}{\nu} \cdot \ln \frac{1}{T_n} \tag{7.6}$$

where

ν = number of sample atoms/barn

F_s = sample area (cm^2)

F_o = flux detector area (cm^2)

ε_{MRD} = $\varepsilon_o \cdot E_B$, E_B being the binding energy of the captured neutrons

TQ = $TQ(T_n, d, r)$ = average transmission of scattered neutrons (d = sample thickness, r = sample radius)

S_γ = self-absorption factor taking into account the capture-γ-ray attenuation by the sample itself.

The calculation of TQ and S_γ will be treated in section X and XI, respectively. It should be noted here that, due to the definition of σ_t according to (7.6), formula (7.4) is also valid for samples of chemical compounds (oxides, carbonates, etc). The only condition which must be fulfilled is that the capture cross sections of the strange atoms are very small compared to the capture cross section σ_c of the element which is to be determined. ν then signifies the number of atoms/barn of that element.

If the element under consideration consists of several isotopes, σ_c in (7.4) has to be replaced by $\overline{\sigma_c} = \Sigma\, a_i \sigma_{c,i}$, a_i being the abundance of the i'th isotope. The counting efficiency of the MRD is then given by

$$\varepsilon_{MRD} = \varepsilon_o \cdot \frac{\Sigma\, a_i \cdot \sigma_{c,i} \cdot E_{B,i}}{\Sigma\, a_i \cdot \sigma_{c,i}} \qquad (7.7)$$

The efficiency thus becomes energy dependent.

For the determination of the isotopic sections $\sigma_{c,i}$ enriched samples are needed (as much different degrees of enrichment as isotopes are present). Then the following equations must be solved by iteration :

$$\begin{pmatrix} \sigma_{c,1} \\ \sigma_{c,2} \\ \cdot \\ \cdot \\ \sigma_{c,k} \end{pmatrix} = \begin{pmatrix} a_{11} & a_{12} & \cdots\cdots & a_{1k} \\ a_{21} & a_{22} & \cdots\cdots & a_{2k} \\ \cdot & & & \cdot \\ \cdot & & & \cdot \\ a_{k1} & a_{k2} & \cdots\cdots & a_{kk} \end{pmatrix}^{-1} * \begin{pmatrix} \overline{\sigma_{c,1}} \\ \overline{\sigma_{c,2}} \\ \cdot \\ \cdot \\ \overline{\sigma_{c,k}} \end{pmatrix} \qquad (7.8)$$

$$\text{with} \quad \overline{\sigma_{c,j}} = \frac{p_j \cdot \sigma_{t,j} \cdot TQ_j}{1 - p_j \cdot (1 - TQ_j)} \qquad (j=1,\ldots,k) \qquad (7.9)$$

$$\text{and} \quad \varepsilon_j = \varepsilon_o \cdot \frac{\Sigma\, a_{ij} \cdot \sigma_{c,i} \cdot E_{B,i}}{\Sigma\, a_{ij} \cdot \sigma_{c,i}} \qquad (7.10)$$

Since the capture-γ-ray spectra of the different isotopes are not equal, the self-absorption factor S_γ is also a function of the sample composition (i.e. of the a_{ij}).

Unfortunately only capture-γ-ray spectra for the natural elements are available up to the present. Thus we have to set $S_{\gamma,j} = S_\gamma$, the self-absorption factor for natural element samples. As it was pointed out elsewhere (4), the error thus introduced is very small provided that $0.9 \leq S_\gamma \leq 1$, a condition which is fulfilled in most of the cases treated in this paper.

If there are two isotopes contained in the element under consideration (k = 2) equation (7.8) can be written

$$\sigma_{c,1} = \frac{1}{DET}\left[a_2 \cdot \overline{\sigma_{c,1}} - (1 - a_1) \cdot \overline{\sigma_{c,2}}\right]$$
$$\sigma_{c,2} = \frac{1}{DET}\left[a_1 \cdot \overline{\sigma_{c,2}} - (1 - a_2) \cdot \overline{\sigma_{c,1}}\right] \qquad (7.11)$$

where $DET = a_1 + a_2 - 1$. Equation (7.10) becomes

$$\varepsilon_1 = \frac{a_1 \cdot \sigma_{c,1} \cdot E_{B,1} + (1-a_1)\sigma_{c,2} \cdot E_{B,2}}{a_1 \cdot \sigma_{c,1} + (1-a_1)\sigma_{c,2}} \cdot \varepsilon_o$$
$$\varepsilon_2 = \frac{(1-a_2)\sigma_{c,1} \cdot E_{B,1} + a_2 \cdot \sigma_{c,2} \cdot E_{B,2}}{(1-a_2)\sigma_{c,1} + a_2 \cdot \sigma_{c,2}} \cdot \varepsilon_o \qquad (7.12)$$

The capture cross sections of ^{151}Eu and ^{153}Eu as well as of ^{175}Lu and ^{176}Lu were determined by iteration using these relations. The initial values for ε_1 and ε_2 were

$$\varepsilon_1 = \left[a_1 E_{B,1} + (1-a_1) E_{B,2} \right] \cdot \varepsilon_o$$

$$\varepsilon_2 = \left[(1-a_2) E_{B,1} + a_2 E_{B,2} \right] \cdot \varepsilon_o \qquad (7.13)$$

For the abundances a_1 and a_2 see Table IV .

If only the capture cross section of the natural element is to be determined and no enriched samples are available, then equation (7.7) must be replaced by approximative expressions :

$$\varepsilon_{MRD} = \varepsilon_o \cdot \frac{\Sigma\, a_i \cdot \sigma^{th}_{c,i} \cdot E_{B,i}}{\Sigma\, a_i \cdot \sigma^{th}_{c,i}} \qquad (7.14)$$

where $\sigma^{th}_{c,i} = \sigma_{c,i}(0.0253\ eV)$, values which are already known with sufficient accuracy for all isotopes reported here. (7.14) is a very good approximation for cross sections which show a nearly 1/v - behaviour (sub-resonance region). In the resonance region ε can be determined by interpolation between some characteristic supporting points :

$$\varepsilon_{peak} = \varepsilon_o \cdot E_{B,i} \qquad (7.15)$$

in those channels where the peak of a resonance of the i'th isotope occurs, and

$$\varepsilon_{valley} = \frac{1}{2} \cdot \varepsilon_o \cdot (E_{B,i} + E_{B,j}) \qquad (7.16)$$

in those channels where the minimum between two resonances (one of the i'th, the other of the j'th isotope) occurs.

If both resonances are of the same isotope, then of course $\varepsilon_{valley} = \varepsilon_{peak}$.

For the evaluation of the Vanadium cross sections only (7.14) was used. For Europium, Dysprosium and Lutetium (7.14) was used in the sub-resonance region and the interpolation method above. In the case of Dysprosium the $\sigma_{c,i}$-values from Danelyan (5) (^{161}Dy, ^{162}Dy, ^{163}Dy) and Sher (6) (^{164}Dy) were used between 0.02 and 1 eV.

These approximation methods for the calculation of the neutron-energy dependent detector efficiency have proved to be very good so that the iteration method for the determination of isotopic cross sections is commonly superfluous.

VIII. BACKGROUND DETERMINATION

The background spectra mentioned in section VI show a smooth shape so that the curves can well be fitted to a three-parameter function of the neutron time-of-flight or the channel number, respectively. The fitted function is used for the normalization described in VI as well as for background subtraction. A maximum accuracy of the background correction is thus attained.

The background spectrum of the MRD observed by means of a boron-carbide filtered beam can be represented by

$$B_{c,1} = C_{11} + C_{12} \cdot \exp(-\Sigma_M D \cdot f(t_{fl})) \qquad (8.1)$$

$$\text{with} \quad f(t_{fl}) = \frac{(D-6h) \cdot \sin\omega t_{fl}}{(D-6h)\sin\omega t_{fl} + 6h}$$

where

Σ_M = average macroscopic cross section of the chopper material for the beam hole background radiation (fast neutrons, γ-rays) detected by the MRD

D = diameter of the chopper rotor

h = slit width (number of slits = 6)

ω = $2\pi f$ = angular frequency of the chopper rotor

t_{fl} = neutron time-of-flight

The parameters C_{11}, C_{12} and Σ_M are determined by means of a least-squares fit. Repeating the measurement with an additional B_4C- filter of the same shape, thickness and density, one obtains

$$B_{c,2} = C_{21} + C_{22} \cdot \exp(-\Sigma_M D \cdot f(t_{fl})) \qquad (8.2)$$

The numbe- of background counts per time channel corresponding to C_{mc} monitor counts can now be written (8.3)

a) no filter :

$$B_c = 2f\Delta C_{mc} \cdot \left[b_{c,1} + b_{c,2} + b_{c,3} \exp(-\Sigma_M D \cdot f(t_{fl})) \right]$$

b) one filter :

$$B_{c,1} = 2f\Delta C_{mc} \cdot \left[b_{c,1} + T_{B,1} \cdot (b_{c,2} + b_{c,3} \exp(-\Sigma_M D \cdot f(t_{fl}))) \right]$$

c) two filters:

$$B_{c,2} = 2f\Delta C_{mc} \cdot \left[b_{c,1} + T_{B,2} \cdot (b_{c,2} + b_{c,3} \exp(-\Sigma_M D \cdot f(t_{fl}))) \right]$$

where

$T_{B,1}$ = transmission of one filter for the beam hole background radiation

$T_{B,2}$ = transmission of the two filters joint in serie ($T_{B,2} = T_{B,1}^2$)

f = chopper frequency (sec^{-1})

Δ = channel width (sec)

By comparison of equations (8.1) and (8.2) with (8.3/b) and (8.3/c) the coefficients $b_{c,i}$ (i=1,2,3) are determined as follows :

$$T_{B,1} = \frac{C_{22}}{C_{12}}$$

$$b_{c,1} = \frac{C_{11}}{2f\Delta C_{mc}} - \frac{C_{22}}{C_{12}} \cdot b_{c,2}$$

$$b_{c,2} = \frac{C_{11}-C_{21}}{C_{12}-C_{22}} \cdot b_{c,3} \qquad (8.4)$$

$$b_{c,3} = \frac{1}{2f\Delta C_{mc}} \cdot \frac{C_{12}}{C_{22}} \cdot C_{12}$$

Since the coefficients $b_{c,i}$ are independent of the chopper frequency as well as of the channel width, they have to be determined only once for a certain sample.

The background for the flux detector is determined analogically. The number of background counts per channel in a flux measurement is given by

$$B_o = 2f\Delta C_{mo} \cdot \left[b_{o,1} + b_{o,2} + b_{o,3} \cdot \exp(-\Sigma_N D \cdot f(t_{fl})) \right] \qquad (8.5)$$

and in a transmission measurement

$$B_t = 2f\Delta C_{mt} \cdot \left[b_{o,1} + T_s \cdot (b_{o,2} + b_{o,3} \cdot \exp(-\Sigma_N D \cdot f(t_{fl}))) \right] \qquad (8.6)$$

where

Σ_N = average macroscopic cross section of the chopper material for the beam hole background radiation detected by the LID

T_s = average transmission of the sample for fast neutrons.

IX. DEAD TIME CORRECTION

In order to get the true counting rates per channel N_c/C_{mc} N_o/C_{mo} and N_t/C_{mt} , the observed counts N_c^*, N_o^* and N_t^* are to be corrected not only for background counts but also for dead time losses. For our TOF-spectrometer the following equations were used :

$$N_c = \frac{N_c^*}{1 - n_c^* \cdot \tau_c} - B_c , \quad n_c^* = \frac{N_c^*}{2f\Delta t_c}$$

$$N_o = \frac{N_o^*}{1 - n_o^* \cdot \tau_o} - B_o , \quad n_o^* = \frac{N_o^*}{2f\Delta t_o} \qquad (9.1)$$

$$N_t = \frac{N_t^*}{1 - n_t^* \cdot \tau_t} - B_t , \quad n_t^* = \frac{N_t^*}{2f\Delta t_t}$$

$$\tau_i = \tau(n_i^*)$$

where t_c, t_o and t_t are the counting times for the capture-, flux- and transmission measurements, respectively. Though the dead time τ is declared by the manufacturer to be fixed for any channel width, it becomes counting rate dependent in the case of high counting rates. The function $\tau(n^*)$ which is needed in (9.1) was determined by means of a new method :

Using a sample material whose energy dependent total cross section is well known, and comparing the measured transmission values with the calculated ones, we obtain

$$T_n = e^{-\nu\sigma_t} = \frac{n_t^*/(1 - n_t^* \cdot \tau(n_t^*)) - B_t}{n_o^*/(1 - n_o^* \cdot \tau(n_o^*)) - B_o} \qquad (9.2)$$

for each channel. The thickness of the sample is chosen so that $0.4 < T_n < 0.6$ over about 100 channels. This can easily be done if the cross section curve shows a smooth shape (for example a 1/v - behaviour). Proceeding from (9.2) the parameters of various functions of the form $\tau(a,b,c,n^*)$ were determined by means of least-squares fits. The best results were obtained with

$$\tau(n^*) = \frac{a}{1 + b \cdot \exp(-c \cdot n^*)} \qquad (9.3)$$

A detailed description of this method is given in (7).

X. MULTIPLE SCATTERING CORRECTION

The effects of single and multiple neutron scattering in samples can be large, even for thin, high-transmission samples. The evaluation of high precision cross sections by means of Monte Carlo calculations are very expensive. For this reason several approximative analytical expressions had been used to compute the necessary corrections (8), (9), (10). The application of those formulae is restricted to relatively thin samples and elements (isotopes) for which

$\sigma_s/\sigma_c \ll 1$. We succeeded in deriving an improved expression with better accuracy which extends the range of application:

Considering a collimated neutron beam incident perpendicularly upon the front face of a sample, the number of capture events per incident neutron is given by

$$\frac{N_c}{N_n} = \frac{\sigma_c}{\sigma_t} \cdot (1-T_n) \cdot f_{sc} \qquad (10.1)$$

f_{sc} being the multiple scattering correction factor due to capture processes following one or several preceding scattering events. As was pointed out elsewhere (11) f_{sc} can be calculated in good approximation by

$$f_{sc} = \frac{1}{TQ + \frac{\sigma_c}{\sigma_t} \cdot (1-TQ)} \qquad (10.2)$$

For a circular disk shaped sample whose diameter is less than the diameter of the neutron beam TQ becomes

$$TQ(T_n,d,r) = \frac{1+2ae^{-a} - e^{-2a}}{4(1-e^{-a})^2} \cdot TQU$$

$$TQU = 1+e^{-w}-e^{-a}-e^{-b}+F(w)-F(a)-F(b)+(w-b)e^{-b(1+z)}$$

$$F(x) = \frac{1}{2} \cdot \left[1-(1+x)e^{-x}+x^2 \cdot EIR(x)\right] \qquad (10.3)$$

$$EIR(x) = \int_x^{\infty} \frac{e^{-t}}{t}\, dt$$

where $a = \ln \frac{1}{T_n}$, $b = \frac{8}{3\pi} \cdot \frac{r}{d} \cdot \ln \frac{1}{T_n}$, $w = \sqrt{a^2+b^2}$

and $z = \frac{a^2}{12 \cdot b^2}$.

Equation (10.3) was derived under the assumption that the neutron velocity is much larger than the average thermal velocity of the target nuclei ($E_n >> kT/A$), so that the target nuclei can be treated as stationary. Furthermore, the sacttering was assumed to be isotropic, which is true for s-wave neutrons scattered from heavy target nuclei ($A >> 1$). Finally, the total cross section for scattered neutrons was considered to be equal to the total cross section for the incident (primary) neutrons in consequence of the relatively small energy loss of a neutron colliding with a heavy nucleus.

The accuracy of equation (10.2) was thoroughly investigated by taking into account the exact geometry of the sample as well as the energy loss of isotropically scattered neutrons (11). It was found that the error of f_{sc} , calculated by (10.2), is less than 1 % for $\nu\sigma_t = \ln(1/T_n) \leqslant 1$ and $d \leqslant r$. Only in the regions of resonance wings, where $\Delta\sigma_t/\sigma_t >> \Delta E_n/E_n$, may the error slightly exceed this value. Formula (10.2) together with (10.3) is thus more accurate than all other analytical expressions reported up to now. Furthermore, it needs much less computer-time than Monte Carlo calculations of the same accuracy.

XI. GAMMA-SELF-ABSORPTION

The thickness of the sample material that can be used is limited also by the self-absorption of capture gamma-rays in the sample. Furthermore, if this absorption becomes large (heavy element samples), the fraction of the γ-rays escaping may become a function of the neutron cross section or the neutron transmission (T_n), respectively. This arises from the fact that a capture event occuring near the front face (which is more likely when the cross section is relatively high) can have an appreciably higher probability of being detected than one that originates in the interior due to the exponential nature of the gamma attenuation. Therefore the calculation of the gamma attenuation factor (S_γ) is very complex. Nevertheless, the determination of this correction is indispensable in the case of low capture cross sections where relatively thick samples are needed in order to get a reasonable captured to incident neutrons ratio.

The data needed for the calculation are

1) the dimensions of the sample and the γ-ray detector (geometric factors)

2) the cross sections for the photon interactions in the sample material (photoelectric interaction, Compton-effect, pair production)

3) the shape of the capture γ-ray spectrum (relative intensities) of the sample material

4) the neutron transmission of the sample.

Since the accuracy of the attenuation factor is determined by the accuracy of these data, it is not necessary to take

into account exactly the geometry of the detector-sample system, which would result in a fourfold integration. We have developed a numerical method for the computation of S_γ being based on a good approximation which only needs double integration. The derivation as well as the accuracy of the formulae given in the following lines are described in detail in (4). The data used were those of Storm et al. (12) for the photon cross sections and those of Rasmussen et al. (13) for the capture γ-ray spectra.

$$S_\gamma = \frac{\sum_{i=1}^{n} h_{\gamma i} \cdot E_{\gamma i} \cdot T_{\gamma i} \cdot K_{\gamma i}}{\sum_{i=1}^{n} h_{\gamma i} \cdot E_{\gamma i}} \tag{11.1}$$

$$T_{\gamma i} = T_\gamma(R, D, \Phi_{eff}, d, \mu_i) \tag{11.2}$$

$$K_{\gamma i} = \left(1 + \sum_{l=1}^{l_{max}} \prod_{j=1}^{l} f_j \cdot k_j\right)_i \tag{11.3}$$

$$T_\gamma(R, D, \Phi_{eff}, d, \mu) = \frac{\alpha/4}{1 - \exp(-\alpha d)} \cdot \frac{I1 + I2}{IG}$$

$$IG = \int_{\varphi_o}^{\pi/2} g(\varphi)\, d\varphi$$

$$I1 = \frac{2}{\mu} \int_{\varphi_o}^{\varphi_*} g(\varphi) \cdot \left[F_1(\varphi, \alpha) + F_1(\varphi, -\alpha) \cdot e^{-\alpha d} \right] d\varphi$$

$$I2 = \frac{2}{\mu} \int_{\varphi_*}^{\pi/2} g(\varphi) \cdot \left[F_2(\varphi,\alpha) + F_2(\varphi,-\alpha) \cdot e^{-\alpha d} \right] d\varphi$$

$$g(\varphi) = \left[\operatorname{arctg} \sqrt{\left(\frac{R}{D}\right)^2 \cdot \sin^2\varphi - \cos^2\varphi} \right] \cdot \sin\varphi \qquad (11.4)$$

$$F_1(\varphi,\alpha) = \frac{\cos\varphi}{a_m} \left[1 - e^{-\alpha d} \cdot e^{-\frac{\mu d}{\cos\varphi}} \right]$$

$$F_2(\varphi,\alpha) = \frac{1}{a_m} \left[\cos\varphi + \frac{\mu}{\alpha} \left(e^{-\frac{\alpha}{2} d^*} - a_m \cdot e^{-\alpha d} \right) \cdot e^{-\frac{\mu \Phi^*}{2 \sin\varphi}} \right]$$

$$a_m = 1 + \frac{\mu}{\alpha} \cdot \cos\varphi \quad , \qquad \Phi^* = \Phi_{eff} = \frac{8}{3\pi} \Phi$$

$$\varphi_* = \operatorname{arctg} \frac{\Phi^*}{2d} \quad , \qquad d^* = \Phi^* \cdot \operatorname{cotg}\varphi$$

$$\varphi_o = \operatorname{arctg} \frac{D}{R} \quad , \qquad \alpha = \frac{1}{d} \ln \frac{1}{T_n}$$

$$\mu = \frac{L}{A} \rho (\sigma_{ph} + \sigma_{co} + \sigma_{pp}) \quad \text{for pure elements}$$

resp. $\frac{L}{M} \rho \sum_k m_k (\sigma_{ph,k} + \sigma_{co,k} + \sigma_{pp,k})$ for chemical compounds (e.g. oxides, carbonates)

$$f_j = (1-TT_{j-1}) \cdot \frac{\sigma_{co,j-1}}{\sigma_{t,j-1}} \cdot \frac{TM_j}{TM_{j-1}} \cdot \frac{E_j}{E_{j-1}} \qquad (11.5)$$

$$k_j = 1 + \frac{\sigma_{pp,j-1}}{\sigma_{co,j-1}} \cdot \frac{0.511}{E_j} \cdot \frac{TM(0.511)}{TM_j} \qquad (11.6)$$

$$E_j = \left(1 - \frac{\sigma_{ab,j-1}}{\sigma_{t,j-1}}\right) \cdot E_{j-1}$$

$$TM_j = T_\gamma(R,D,\Phi_{eff},d,\mu_j)$$

$$TT_j = T_\gamma(R,D,\Phi_{eff},d,\mu_j) \text{ with } \varphi_o=0 \text{ and } g(\varphi)=\sin\varphi$$

$$\sigma_{ph,j} = \sigma_{ph}(E_j) \quad / \quad \sigma_{co,j} = \sigma_{co}(E_j)$$
$$\sigma_{pp,j} = \sigma_{pp}(E_j) \quad / \quad \sigma_{ab,j} = \sigma_{ab}(E_j)$$
$$\sigma_{t,j} = \sigma_{ph,j} + \sigma_{co,j} + \sigma_{pp,j} \quad / \quad \mu_j = \mu(E_j)$$

The capture-γ-ray spectrum is given by $h_{\gamma i}(E_{\gamma i})$, $(i=1,\ldots,n)$ where $E_{\gamma i}$ = capture-γ-ray energy and $h_{\gamma i}$ = relative intensity. $T_{\gamma i}$ is the probability for a γ-ray of energy $E_{\gamma i}$ escaping into the sensitive detector solid angle and $K_{\gamma i}$ is a factor taking into account multiple Compton scattering.

The parameters characterizing the geometry of the detector-sample system are

Φ = sample diameter
d = sample thickness
R = scintillator radius (MRD)

D = distance between the center of the sample and the scintillators of the detector.

The interaction cross sections used are

σ_{ph} = total photoelectric cross section

σ_{co} = total incoherent bound electron scattering cross section

σ_{pp} = total pair production cross section

σ_{ab} = absorption cross section of the incoherent bound electron interaction.

The index j signifies the order of multiple scattering radiation, j = 0 relates to the original capture gamma radiation so that $E_o \equiv E_{\gamma i}(MeV)$, $\mu_o \equiv \mu_i$, $TM_o \equiv T_{\gamma i}$, $\sigma_{ph,o} \equiv \sigma_{ph}$ and so on. TT_j is the total escape probability for a γ-ray of energy E_j and is calculated by setting $\varphi_o = 0$ and $g(\varphi) = \sin\varphi$ as well as $\mu = \mu_j$ in the formulae for $T_\gamma(R,D,\Phi_{eff},d,\mu)$.

For the calculation of the attenuation coefficients μ_i resp. μ_j the following additional quantities are needed :

ρ = density of the sample material

A = atomic weight of the sample atoms

M = molecular weight of the sample molecules

m_k = number of atoms of the kind k per molecule

L = Avogadro's constant.

The parameter l_{max} in (11.3) is chosen so that the term

$$\prod_{j=1}^{l_{max}} f_j \cdot k_j < 10^{-4} .$$

It should be noted here that the same formulae with only slight modifications are applicable to liquid-scintillator-tank detectors ($\varepsilon \sim 100$ %) :

$$S_\gamma = \frac{\sum_{i=1}^{n} h_{\gamma i} \cdot T_{\gamma i} \cdot K_{\gamma i}}{\sum_{i=1}^{n} h_{\gamma i}} \tag{11.7}$$

$$T_{\gamma i} = T_\gamma(\Phi_{eff}, d, \mu_i) \tag{11.8}$$

with $\varphi_o = 0$, $g(\varphi) = \sin\varphi$ (11.9)

and $$f_j = (1-TT_j) \cdot \frac{\sigma_{co,j-1}}{\sigma_{t,j-1}} \cdot \frac{TT_j}{TT_{j-1}} \tag{11.10}$$

$$k_j = 1 + \frac{\sigma_{pp,j-1}}{\sigma_{co,j-1}} \cdot \frac{TT(0.511)}{TT_j} \quad . \tag{11.11}$$

Another equation, which was found to be very useful in order to reduce considerably the computing time in the cross section evaluation according to (7.4), relates to the neutron transmission dependence of the attenuation factor : For a given sample $S_\gamma(T_n)$ can well be fitted to a rational function of the form

$$S_\gamma = \frac{a + b \cdot T_n}{1 + c \cdot T_n} \quad . \tag{11.12}$$

The results obtained by means of these formulae were checked by measuring some well known thermal capture cross sections with samples of various thicknesses and comparing with the

true values. Within the error limits of the latter ($\pm$ 1.2 % to $\pm$ 1.7 %) conformity was ascertained for attenuation factors between 0.7 and 1 .

XII. SAMPLE ACTIVATION

In some cases the activation of the sample during neutron irradiation may contribute to the background rate of the capture detector. If the decay time of the produced radioactive isotope is essentially greater than the counting time in the capture cross section measurement this contribution can easily be determied by measuring the background rate with closed beam channel (room background) immediately before and afterwards. For short decay times the determination of the background correction in question is more difficult.

The method we used is applicable to both cases, very simple and of sufficient accuracy. First, the background parameters described in section VIII were determined before the capture measurement concerned. The calculated background counts (according to (8.3/a)) were then compared to the measured true background counts in the last 50 channels of the time-of-flight spectrum (section VI). If the average true background rate exceeds the calculated one by more than 5 %, this is due to sample activation as has been checked by several test measurements. Since the contribution of the activation is not energy dependent (resp. time-of-flight dependent), formula (8.3/a) can be made correct by increasing the parameter $b_{c,1}$ so that the calculated average becomes equal to the above mentioned true average.

XIII. NEUTRON ENERGY

The neutron energy corresponding to the i'th time channel is given by

$$E_{n,i} = \frac{k}{t_{fl,i}^2} \quad [eV] \qquad (13.1)$$

with $t_{fl,i} = \Delta \cdot i + \tau_t$

and $\tau_t = \tau_o + \tau_d - \Delta/2$

where

$t_{fl,i}$ = neutron time-of-flight (μs)

Δ = channel width (μs)

τ_d = adjusted delay of the start-pulses (μs)

τ_o = delay time correction due to cables, amplifiers and pulse shape circuits (μs)

The constant k was determined by measuring and analyzing the peaks of several well resolved resonances whose energies are well known. The value thus obtained $(1.230 \pm 0.0025) \cdot 10^6$ was in good agreement with the corresponding, independently measured, flight-path length of 15.340 ± 0.015 metres. Table III shows the characteristic parameters of the measured time-of-flight spectra, where

f = chopper frequency (revolutions per second)

E_{co} = neutron cut-off energy of the chopper

n_{ch} = number of channels per spectrum.

The values for f, Δ, τ_d and n_{ch} were adjusted, those of τ_o measured and those of E_{co} calculated (XV/2).

TABLE III

Time-of-flight spectrum parameters

f	E_{co}	τ_d	Δ	τ_o	n_{ch}
25 c/s	0.008 eV	7•256 μs	128/64 μs	+5.1 μs	128/256
50	0.032	7•128	64/32	+2.1	128/256
100	0.128	7•64	16	+0.6	256
200	0.512	7•32	8/4	-0.1	256/512
400	2.048	7•16	4/2	-0.5	256/512

XIV. SAMPLES USED

The characteristic properties of the samples used in the capture cross section measurements reported here are listed in Table IV. The oxide- and carbonate-samples consisted of pressed powder disks. In order to get homogeneous samples, uniform in thickness and of good stability, different pressures had to be used. For this reason different densities were obtained. The marked samples (*) were enclosed in thin-wall, vacuum-tight canisters of pure aluminum (thickness 0.3 mm). Measurements carried out with and without an empty canister in sample position showed that the contribution due to captures in the canister material could be neglected. The influence of the canister material on the neutron transmission of a sample was eliminated by using an empty canister as dummy sample in the corresponding flux measurements.

For the measurement of the high Europium cross sections below 0.6 eV a very thin sample was needed. To get a reasonable, uniform thickness a small amount of Eu_2O_3-powder (0.5 g) was well mixed and thus diluted with sulphur-powder

TABLE IV Specification of samples

element/ isotope	isotopic composition	chemical form	density g/ccm	diameter cm	thickness cm	atoms/barn
Vanadium	0.24 % ^{50}V	metallic	6.11	3.92	0.965	$6.968 \cdot 10^{-2}$
(nat.)	99.76 % ^{51}V	metallic	6.12	3.92	0.930	$6.925 \cdot 10^{-2}$
Manganese	100 % ^{55}Mn	metallic	7.16	3.79	1.020	$7.984 \cdot 10^{-2}$
Cesium	100 % ^{133}Cs	Cs_2CO_3 *)	3.03	3.80	0.140	$1.570 \cdot 10^{-3}$
(nat.)	100 % ^{133}Cs	Cs_2CO_3 *)	3.87	3.81	0.830	$1.187 \cdot 10^{-2}$
Europium	47.82 % ^{151}Eu	Eu_2O_3 + S	1.72	3.81	0.230	$1.505 \cdot 10^{-4}$
(nat.)	52.18 % ^{153}Eu	Eu_2O_3	2.67	3.81	0.145	$1.327 \cdot 10^{-3}$
^{153}Eu	99.2 % ^{153}Eu	Eu_2O_3 *)	3.03	3.82	0.165	$1.701 \cdot 10^{-3}$
(enr.)	0.8 % ^{151}Eu					
Dysprosium	nat. element	Dy_2O_3	3.97	3.80	0.135	$1.730 \cdot 10^{-3}$
(nat.)		Dy_2O_3	3.99	3.81	0.450	$5.806 \cdot 10^{-3}$
Lutetium	97.41 % ^{175}Lu	Lu_2O_3 *)	3.83	3.81	0.260	$3.017 \cdot 10^{-3}$
(nat.)	2.59 % ^{176}Lu	Lu_2O_3 *)	2.61	3.81	1.680	$1.328 \cdot 10^{-2}$
^{175}Lu	99.77 % ^{175}Lu	Lu_2O_3 *)	3.49	3.81	0.285	$3.008 \cdot 10^{-3}$
(enr.)	0.23 % ^{176}Lu					
Tantalum	99.988 % ^{181}Ta	metallic	16.30	3.80	0.104	$5.617 \cdot 10^{-3}$
(nat.)	0.012 % ^{180}Ta	metallic	16.30	3.80	0.233	$1.264 \cdot 10^{-2}$
		metallic	15.75	3.92	0.984	$5.157 \cdot 10^{-2}$

(4 g). This mixture could easily be pressed to a disk shaped tablet. Since the capture cross section of sulphur is very small compared to the Europium cross section, its contribution to the counting rate of the capture detector is completely negligible. However, the influence on the multiple scattering correction (neutron scattering cross section) as well as the self-absorption factor (γ-attenuation coefficient) has to be taken into account.

The values listed in the last column of the table indicate the number of atoms/barn of the element whose capture cross section has been determined (e.g. number of Cs-atoms in the Cs_2CO_3-sample or number of Eu-atoms in the Eu_2O_3-sample etc.).

For the sample preparation only high-purity materials were used. The contributions of the "strange atoms" were estimated and found to be negligible. Thus, no corrections for impurities were applied.

XV. ERROR ANALYSIS

1. Energy Scale

According to equation (13.1) the relative energy error becomes

$$\frac{\Delta E_n}{E_n} = \sqrt{\left(\frac{\Delta k}{k}\right)^2 + \left(2\cdot\frac{\Delta t_{fl}}{t_{fl}}\right)^2}$$

Since k was measured by means of relatively thin samples and

$$k = \frac{1}{2}\cdot m_n\cdot L^2$$

m_n being the neutron mass and L the flight path length, $\Delta k/k$ has to be replaced by the term

$$(2\cdot\Delta L/L)^2 + (d/L)^2$$

if thick samples are used (d = sample thickness). Δt_{fl} is given by

$$\Delta t_{fl} = \Delta\tau_t = \Delta\tau_o$$

$\Delta\tau_o$ being the time jitter of the stop-pulses relative to the start-pulses, the measured values of which are listed in Table V. The errors of Δ and τ_d are less than 0.01 % and were therefore neglected.

The error of the neutron energy thus becomes

$$\frac{\Delta E_n}{E_n} = \sqrt{A + B\cdot E_n} \qquad (15.1)$$

where $A = 4\cdot(\Delta L/L)^2 + (d/L)^2$ and $B = \frac{4}{k}(\Delta\tau_o)^2$.

TABLE V

Measured time jitters

$f_{chopper}$	jitter of start-pulses	jitter of stop-pulses	$\Delta\tau_o$
25 c/s	± 1.0 μs	± 0.05 μs	± 1.0 μs
50	0.5	0.05	0.5
100	0.25	0.05	0.25
200	0.12	0.05	0.13
400	0.06	0.05	0.08

2. Energy Resolution

The measured cross section curves are broadened not only by the Doppler effect but also by the instrumental resolution. The total resolution function is a convolution of partial resolution functions describing the effects of neutron burst width, channel width and time jitter.

The neutron burst can be represented by a triangular distribution whose base-width τ_b is given by

$$\tau_b = \sqrt{\frac{1 - \frac{128}{5}\beta^4}{1 - \frac{8}{3}\beta^2}} \cdot \frac{h}{\omega R} \qquad \text{for } 0 \leq \beta \leq 1/4$$

$$\tau_b = \sqrt{\frac{3}{5} \cdot \frac{(4-\beta-3\sqrt{\beta})(\sqrt{\beta}-\beta)^3}{\beta^2-3\beta+2\sqrt{\beta}}} \cdot \frac{4h}{\omega R} \qquad \text{for } 1/4 \leq \beta \leq 1$$

with $\beta = \sqrt{\frac{E_{co}}{E_n}}$

and $E_{co} = \frac{m_n}{2} \cdot \left(\frac{\omega R^2}{h}\right)^2 = k \cdot \left(\frac{\omega R^2}{hL}\right)^2$

where

ω = $2\pi f$ (chopper frequency)

h = slit width

R = chopper radius

L = flight-path length

E_{co} = cut-off energy

For $E_n \leqslant E_{co}$ $(\beta \geqslant 1)$ the neutron transmission of the chopper is naught.

The influence of the analyzer-channel width (Δ) as well as the time jitter are described by rectangular distributions. The width of the time jitter is given by $\tau_j = 2 \cdot \Delta\tau_o$. In the case of thick samples an additional broadening effect is to be considered, a rectangular distribution of the width

$$\tau_L = \frac{d}{L} \cdot t_{fl} \qquad \text{(depth effect)} .$$

The convolution of all these partial resolution functions can be represented in good approximation by a Gaussian distribution whose full width at half maximum (FWHM) becomes

$$\Delta t_{FWHM} = \sqrt{\frac{2}{3} \ln 2} \cdot \sqrt{\Delta^2 + \frac{1}{2} \cdot \tau_b^2 + \tau_j^2 + \tau_L^2} \qquad (15.3)$$

$$\frac{\Delta t_{FWHM}}{t_{fl}} = \sqrt{\frac{2}{3} \ln 2} \cdot \sqrt{\left(\frac{\Delta}{t_{fl}}\right)^2 + \frac{1}{2}\left(\frac{\tau_b}{t_{fl}}\right)^2 + 4\left(\frac{\Delta\tau_o}{t_{fl}}\right)^2 + \left(\frac{d}{L}\right)^2}$$

The corresponding total energy resolution is then

$$res(E_n) = 2 \frac{\Delta t_{FWHM}}{t_{fl}} E_n \qquad (15.4)$$

and the resolution in μs/metre : $\Delta t_{FWHM}/L$.

3. Systematic Errors

In this section the formulae used for the calculation of the sytematic errors of the measured capture cross sections are given. They were derived by consistently applying the law of error propagation to the relationships of section V and VII. Sources of small errors which have no influence on the total error were neglected.

$$\left(\frac{\Delta\sigma_c}{\sigma_c}\right)^2_{sys} = \left(\frac{\Delta\nu}{\nu}\right)^2 + \left(1 + \frac{1-TQ}{TQ}\cdot\frac{\sigma_c}{\sigma_t}\right)^2 \cdot \left(\frac{\Delta p}{p}\right)^2_{sys} + \left(\frac{\Delta f_{sc}}{f_{sc}}\right)^2_{appr.}$$

$$\left(\frac{\Delta p}{p}\right)^2_{sys} = \left(\frac{\Delta\Phi_n}{\Phi_n}\right)^2_{sys} + \left(\frac{\Delta F_s}{F_s}\right)^2 + \left(\frac{\Delta\varepsilon_{MRD}}{\varepsilon_{MRD}}\right)^2 + \left(\frac{\Delta S_\gamma}{S_\gamma}\right)^2 \qquad (15.5)$$

$$\left(\frac{\Delta\Phi_n}{\Phi_n}\right)^2_{sys} = \left(\frac{\Delta F_o}{F_o}\right)^2_{sys} + \left(\frac{\Delta f_{so}}{f_{so}}\right)^2 + \left(\frac{\partial\Phi_n}{\partial c_1}\cdot\frac{\Delta c_1}{\Phi n}\right)^2 + \left(\frac{\partial\Phi_n}{\partial c_2}\cdot\frac{\Delta c_2}{\Phi_n}\right)^2 + \left(\frac{\partial\Phi_n}{\partial E_n}\cdot\frac{\Delta E_n}{\Phi_n}\right)^2$$

The calculated resp. estimated values for the particular components are

$$\frac{\Delta\nu}{\nu} = \frac{\Delta F_s}{F_s} = \frac{\Delta F_o}{F_o} = 0.5\ \%$$

$$\left(\frac{\Delta f_{sc}}{f_{sc}}\right)_{appr.} = 1\ \% \quad , \quad \left(\frac{\Delta f_{so}}{f_{so}}\right)_{appr.} = 0.2\ \%$$

$$\frac{\Delta \varepsilon_{MRD}}{\varepsilon_{MRD}} = \frac{\Delta \varepsilon_{o}}{\varepsilon_{o}} = 1.2\ \%$$

$$\frac{\Delta S_{\gamma}}{S_{\gamma}} = \sqrt{10(1-S_{\gamma})} \cdot 10^{-2} \qquad \text{for} \quad 0.5 \leqslant S_{\gamma} \leqslant 0.9$$

$$= 1\ \% \qquad \text{for} \quad 0.9 \leqslant S_{\gamma} \leqslant 1$$

$$\left(\frac{\Delta \Phi_{n}}{\Phi_{n}}\right)_{sys} = (6.219 + 0.1698 \cdot \ln E_{n}) \cdot 10^{-3}$$

4. Statistical Errors

The statistical errors of the measured capture cross sections were determined according to the following relationships :

$$\left(\frac{\Delta \sigma_{c}}{\sigma_{c}}\right)^{2}_{stat} = \left[\frac{T_{n}}{1-T_{n}}\left(1+\frac{1-TQ}{TQ}\cdot\frac{\sigma_{c}}{\sigma_{t}}\right) + \frac{1}{\ln Tn} - \left(1-\frac{\sigma_{c}}{\sigma_{t}}\right)\cdot\frac{1}{TQ}\cdot\frac{\partial TQ}{\partial a}\right]^{2} \cdot$$

$$\cdot\left[\left(\frac{\Delta N_{o}}{N_{o}}\right)^{2} + \left(\frac{\Delta N_{t}}{N_{t}}\right)^{2}\right] + \left(1+\frac{1-TQ}{TQ}\cdot\frac{\sigma_{c}}{\sigma_{t}}\right)^{2}\cdot\left(\frac{\Delta N_{c}}{N_{c}}\right)^{2} \qquad (15.6)$$

$$\frac{\partial TQ}{\partial a} = \frac{1+2ae^{-a} - e^{-2a}}{4(1-e^{-a})^{2}} \cdot \left[e^{-a} + \frac{b}{a}e^{-b} - \frac{w}{a}e^{-w} - \ldots\right.$$

$$\ldots -a\cdot EIR(a)+\frac{w^2}{a}\,EIR(w)-\frac{b^2}{a}\,EIR(b)+\frac{w-b}{a}(1-u)e^{-u}\Big] -$$

$$-\frac{2ae^{-a}(1+e^{-a})}{(1-e^{-a})(1+2ae^{-a}-e^{-2a})}\cdot TQ$$

where $u = b\cdot(1+z)$ (for a,b,w and z see section X)

and
$$\frac{\Delta N_o}{N_o} = \frac{k_o\cdot\sqrt{N_o^*}}{k_o\cdot N_o^* - B_o}\,, \qquad k_o = \frac{1}{1-n_o^*\cdot\tau_o}$$

$$\frac{\Delta N_t}{N_t} = \frac{k_o\cdot\sqrt{N_t^*}}{k_t\cdot N_t^* - B_t}\,, \qquad k_t = \frac{1}{1-n_t^*\cdot\tau_t} \qquad (15.7)$$

$$\frac{\Delta N_c}{N_c} = \frac{k_c\cdot\sqrt{N_c^*}}{k_c\cdot N_c^* - B_c}\,, \qquad k_c = \frac{1}{1-n_c^*\cdot\tau_c}$$

k_o , k_t , k_c being the dead time correction factors.

Most of the capture cross sections were measured independently several times so that the errors of the quoted average values are reduced by a factor $1/\sqrt{n}$, n being the number of measurements.

5. Total Errors

The total error of a capture cross section value is given by

$$\left(\frac{\Delta\sigma_c}{\sigma_c}\right)^2_{tot} = \left(\frac{\Delta\sigma_c}{\sigma_c}\right)^2_{sys} + \left(\frac{\Delta\sigma_c}{\sigma_c}\right)^2_{stat} \qquad (15.8)$$

In calculating the cross sections of the pure isotopes of sample materials containing two different isotopes according to (7.11), the errors of the evaluated values are found by means of

$$\Delta\sigma_{c,1} = \frac{1}{DET} \cdot \sqrt{a_2^2 \cdot \left(\Delta\overline{\sigma_{c,1}}\right)^2 + \left(1-a_1\right)^2 \cdot \left(\Delta\overline{\sigma_{c,2}}\right)^2}$$

$$\Delta\sigma_{c,2} = \frac{1}{DET} \cdot \sqrt{\left(1-a_2\right)^2 \cdot \left(\Delta\overline{\sigma_{c,1}}\right)^2 + a_1^2 \cdot \left(\Delta\overline{\sigma_{c,2}}\right)^2} \qquad (15.9)$$

with $DET = a_1 + a_2 - 1$.

These relations hold for the total systematic, the total statistical as well as the total total error.

XVI. RESULTS AND CONCLUSIONS

The energy dependent capture cross sections obtained in this work are shown in the Figures 4 through 16. The measured values are represented by points, the fitted cross section curves by solid lines.

The cross sections for the pure isotopes ^{151}Eu, ^{153}Eu, ^{175}Lu and ^{176}Lu were derived from the fitted curves of the natural element cross sections and the enriched isotope cross sections. Here, the solid lines indicate the upper and the lower limits of the total error, respectively.

The shape of the Vanadium cross section curve shows a pure 1/v-behaviour as could be expected from the known positive

energy resonances. No contribution of any negative energy level (bound level) can be substantiated.

The small but significant hump observed at 0.43 eV in the Tantalum cross section curve is due to the 0.43 eV - resonance of ^{180}Ta whose natural abundance amounts to only 0.012 % .

The shapes of the other capture cross section curves show no special peculiarities compared with the already known total cross section curves, except the essentially lower values between the resonances.

The accuracy attained for the capture cross section values is 2 - 4 % from 0.01 to 1 eV (2 % in the thermal region) and 3 - 5 % above 1 eV. For some resonance cross sections above 4 eV the total error increases up to 10 %.

Thus, the magnitudes of the capture cross sections have been obtained with appreciably smaller errors than were reported previously, which illustrates the utility of the new methods applied for the flux measurement, the determination of background and dead time losses as well as for the calculation of the multiple-scattering and gamma-self-absorption correction.

All data, incl. systematic and statistical errors, have been transmitted to the NEA Neutron Data Compilation Centre in Saclay, France, and are available on request.

ACKNOWLEDGEMENTS

The author would like to acknowledge the assistance of E. HERMES in sample preparation and in the construction of the mechanical installations, and of K. BEHRINGER, J. PHILDIUS and B. LEONI in electronic apparatus fabrication.

REFERENCES

(1) K. Behringer, B. Leoni and J. Phildius, EIR-TM-PH-465 (1973) and EIR-TM-PH-481 (1973)

(2) E. Hermes, F. Widder and P. Keller, EIR-TM-PH-483 (1973)

(3) F. Widder, EIR-TM-PH-314 (1969)

(4) F. Widder, EIR-TM-PH-490 (1973)

(5) L.S. Danelyan, Atomnaya Energiya 16 (1964) 56

(6) R. Sher, S. Tassan, E.V. Weinstock and A. Hellsten, Nucl. Sci. Eng. 11 (1961) 369

(7) F. Widder, EIR - Bericht Nr. 216 (1972)

(8) H.W. Schmitt, ORNL - 2883 (1960)

(9) R.L. Macklin, Nucl. Instr.Meth. 26 (1964) 213

(10) S.J. Friesenhahn, E. Haddad, F.H. Fröhner and W.M. Lopez, Nucl. Sci. Eng. 26 (1966) 487

(11) F. Widder, EIR-TM-PH-453 (1972)

(12) E. Storm and H.I. Isreal, LA - 3753 (1967)

(13) N.C. Rasmussen, V.J. Orphan, T.L. Harper, J. Cunningham and S.A. Ali, DASA - 2570 (1970)

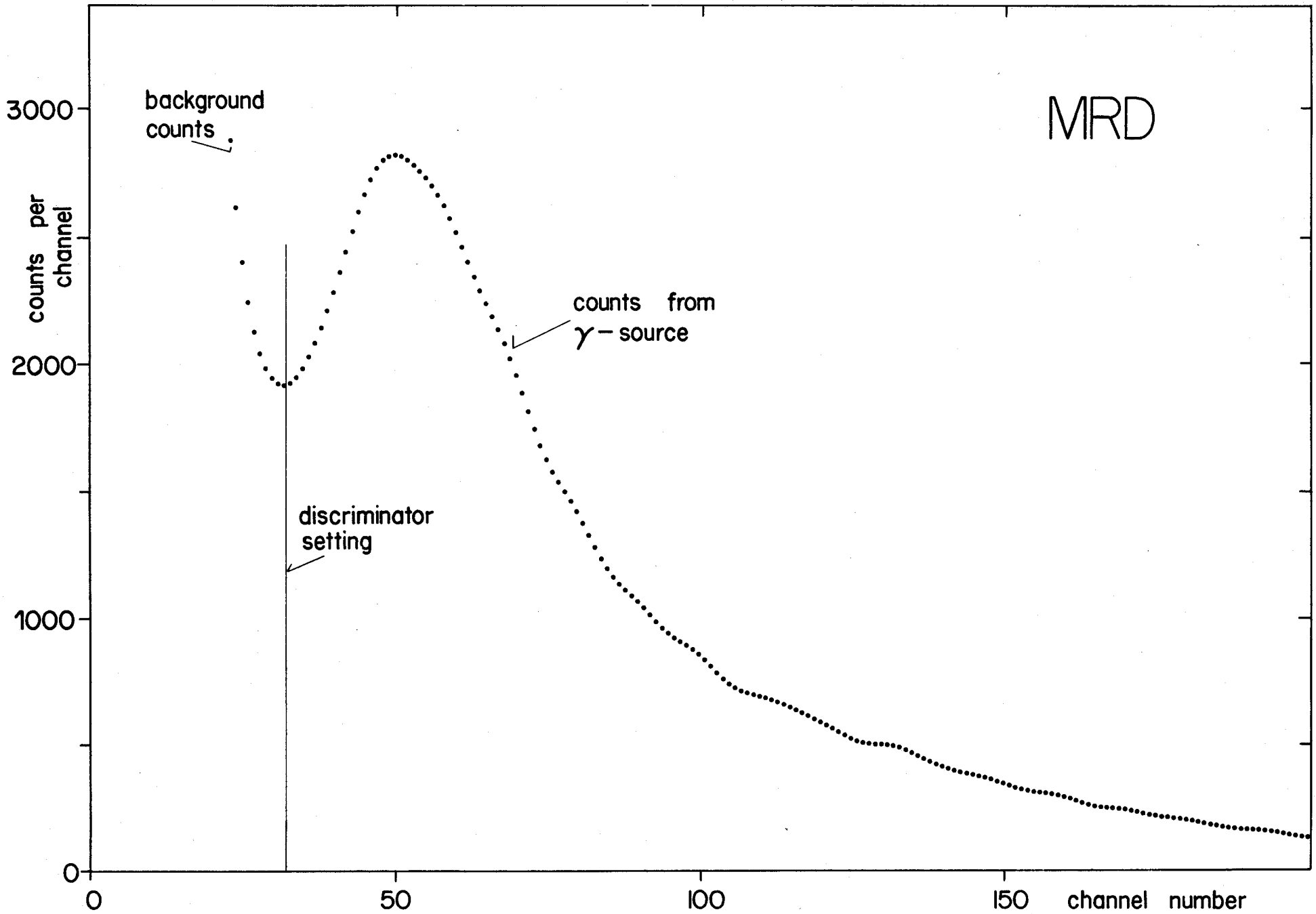

FIG.1 PULSE HEIGHT DISTRIBUTION OF THE MOXON-RAE DETECTOR

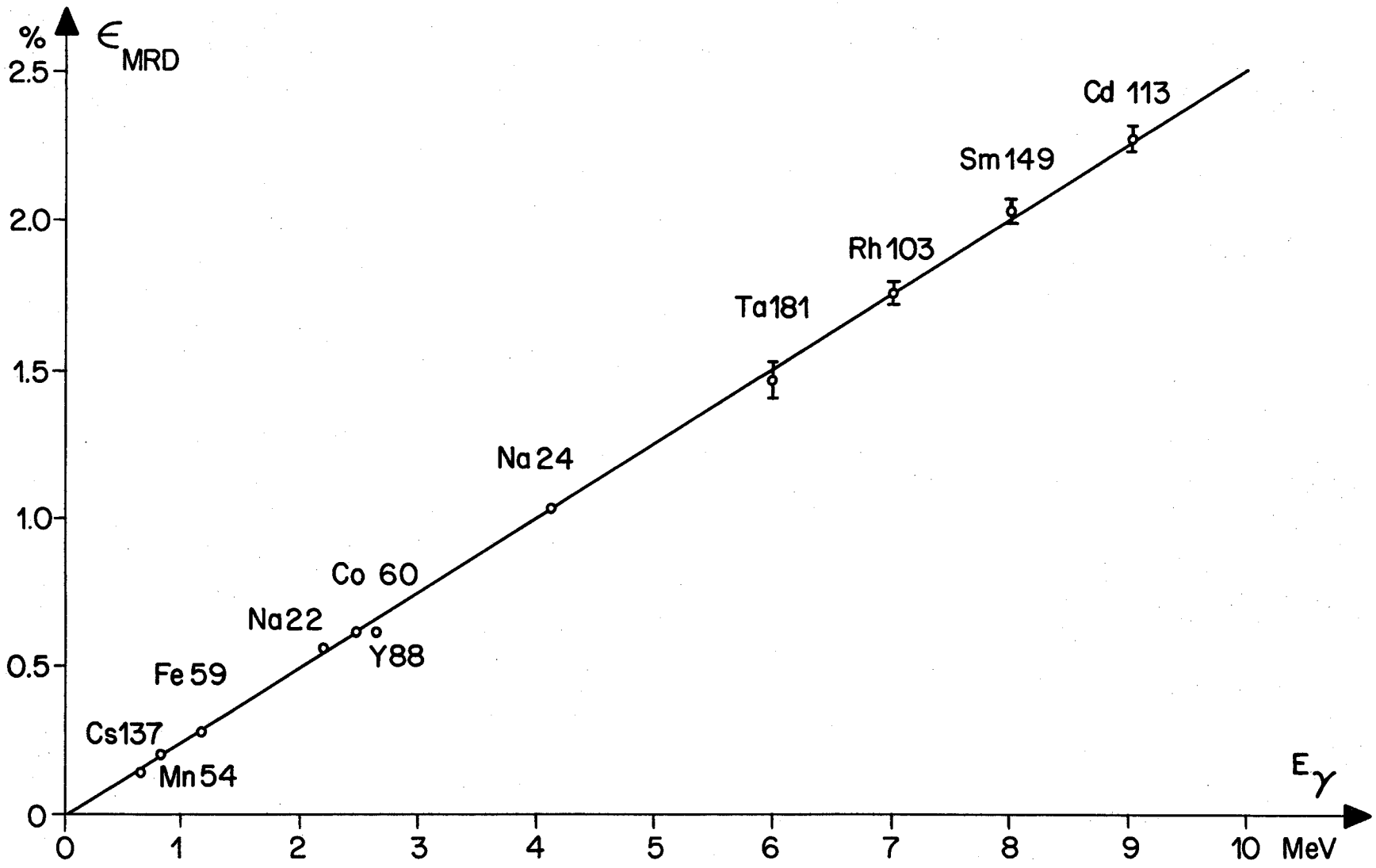

FIG. 2 DETECTION EFFICIENCY OF THE MRD

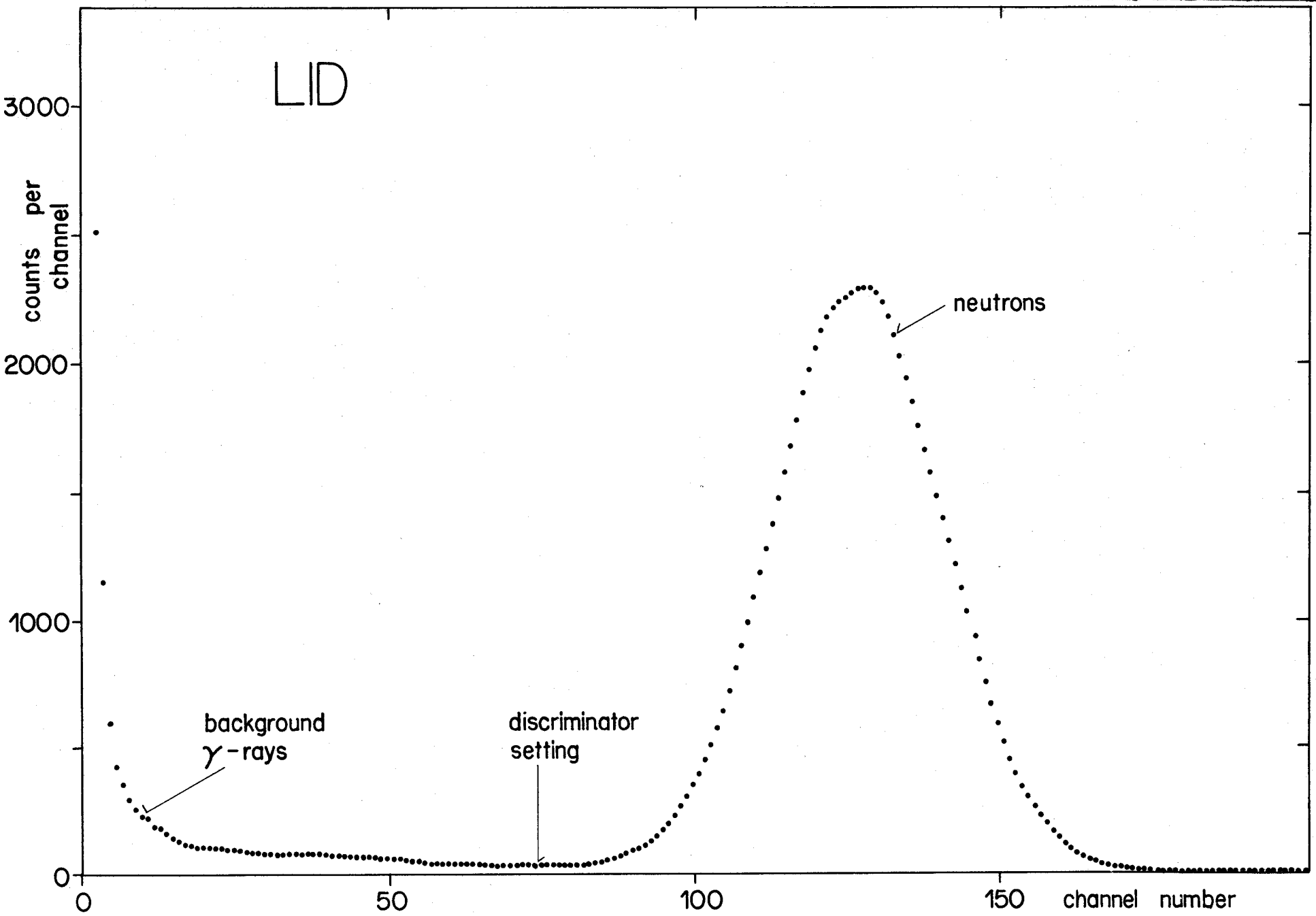

FIG.3 RESPONSE CURVE OF THE NEUTRON FLUX DETECTOR

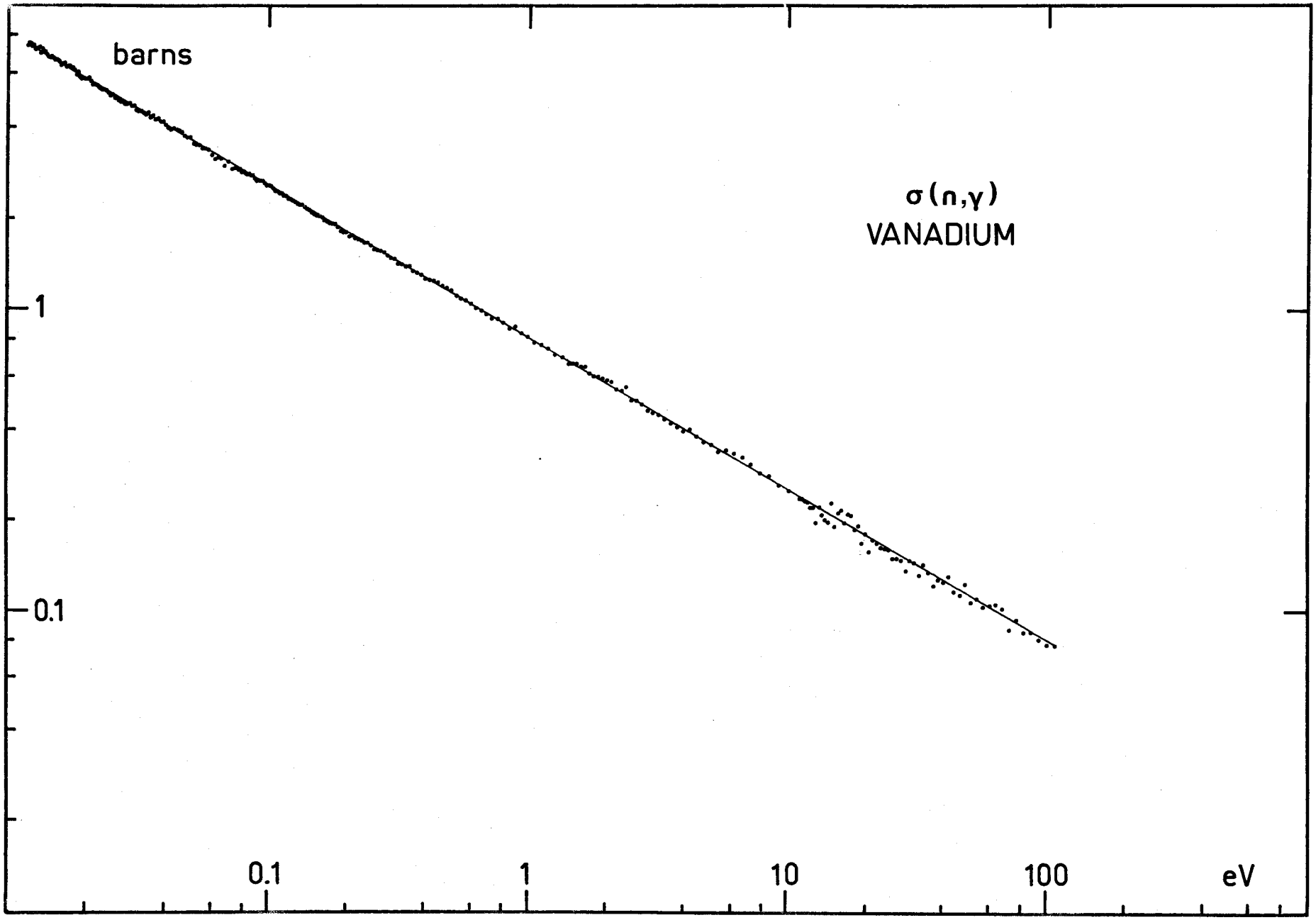
barns
σ(n,γ)
VANADIUM
1
0.1
0.1
1
10
100
eV

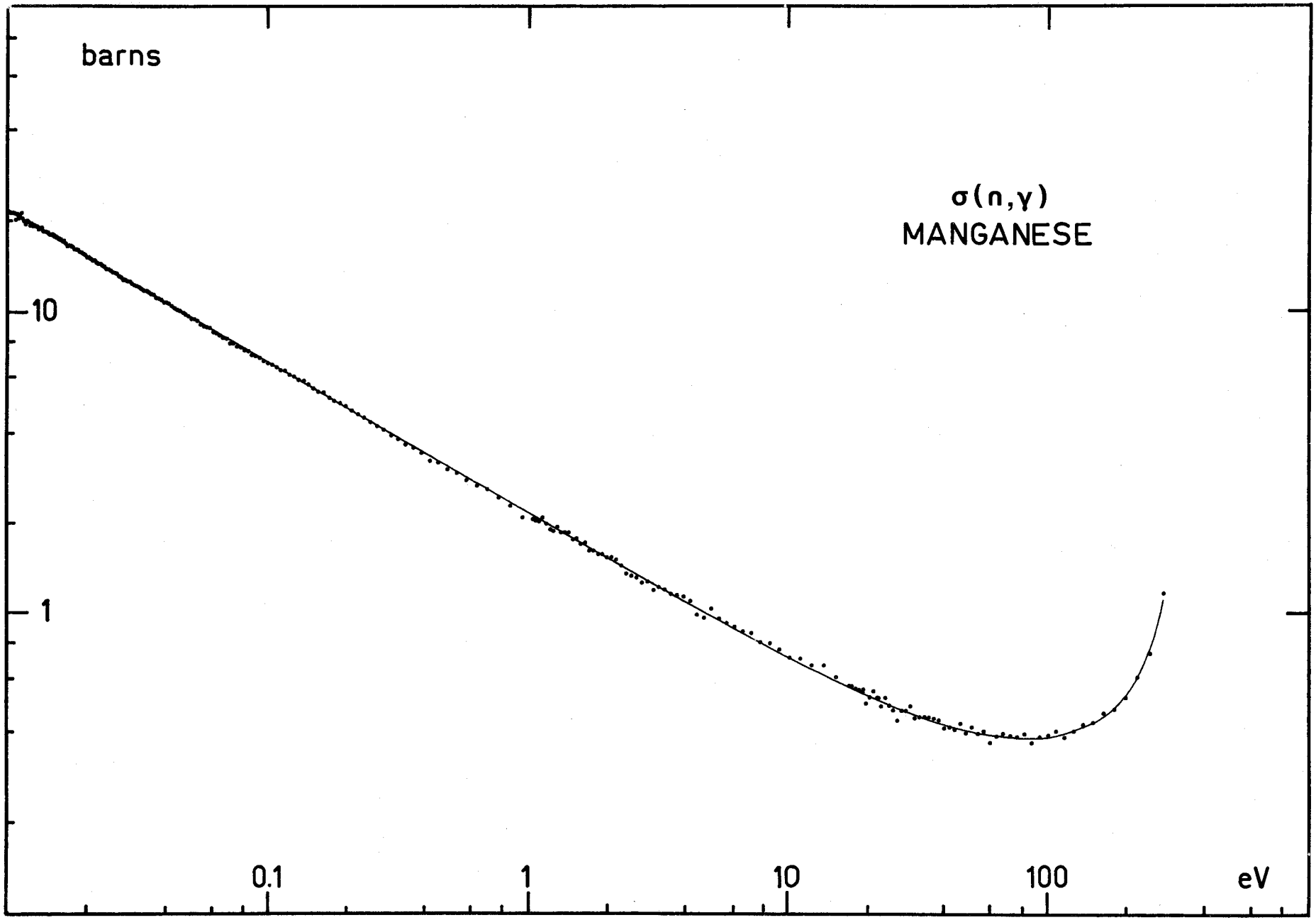
barns
σ(n,γ)
MANGANESE
10
1
0.1
1
10
100
eV

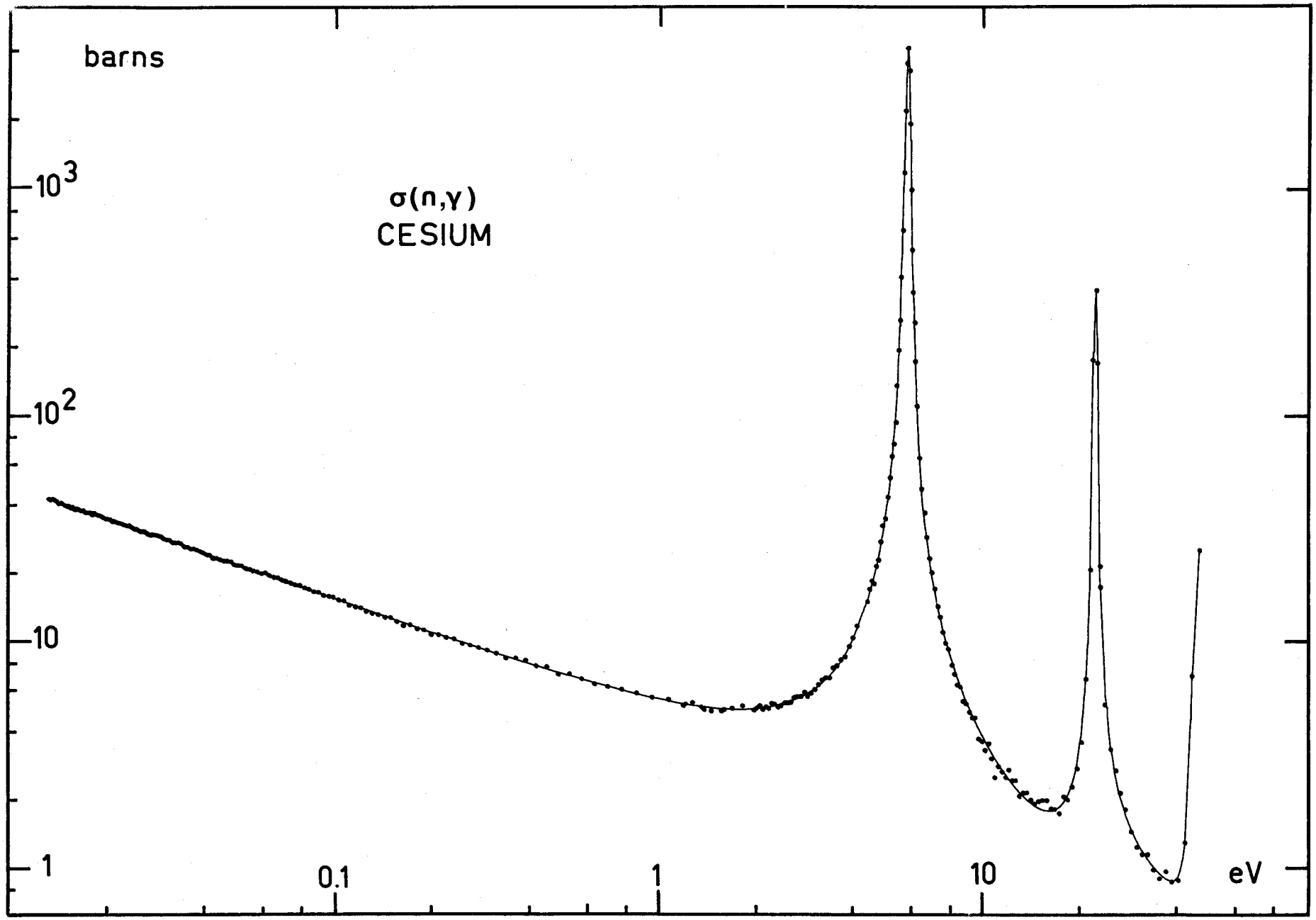
barns
σ(n,γ)
CESIUM
10^3
10^2
10
1
0.1
1
10
eV

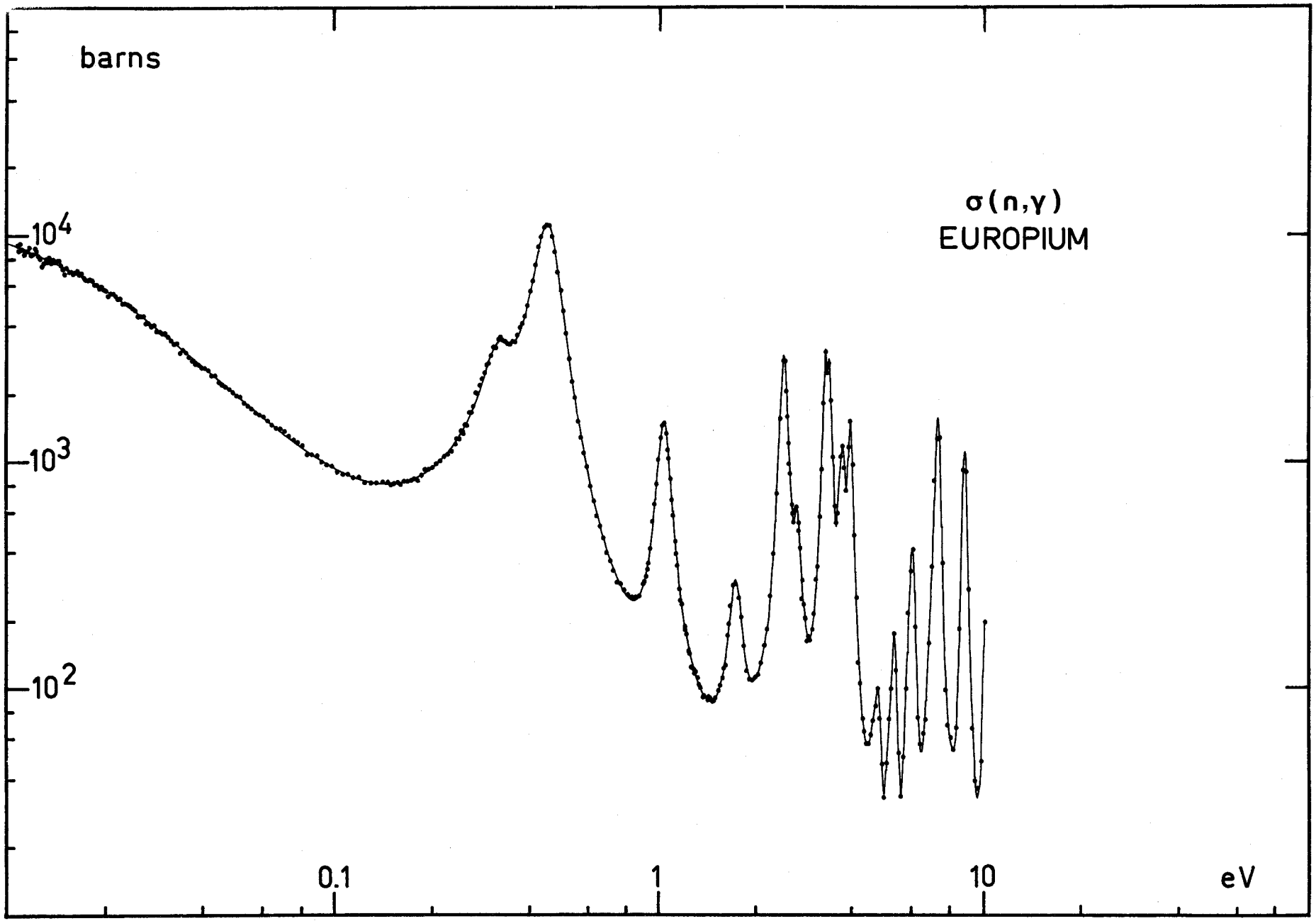
barns
σ(n,γ)
EUROPIUM
10^4
10^3
10^2
0.1
1
10
eV

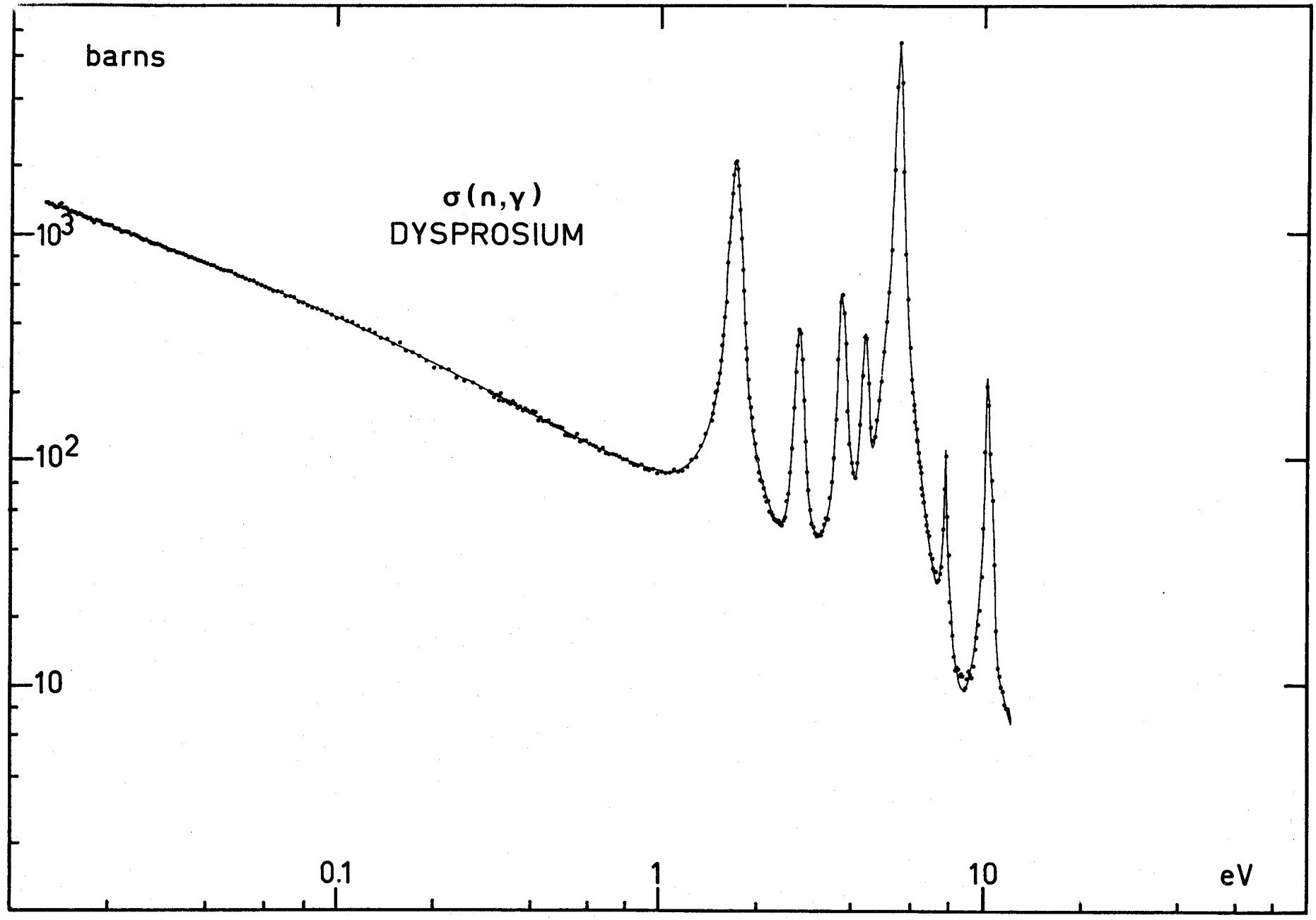
barns
σ(n,γ)
DYSPROSIUM
10³
10²
10
0.1
1
10
eV

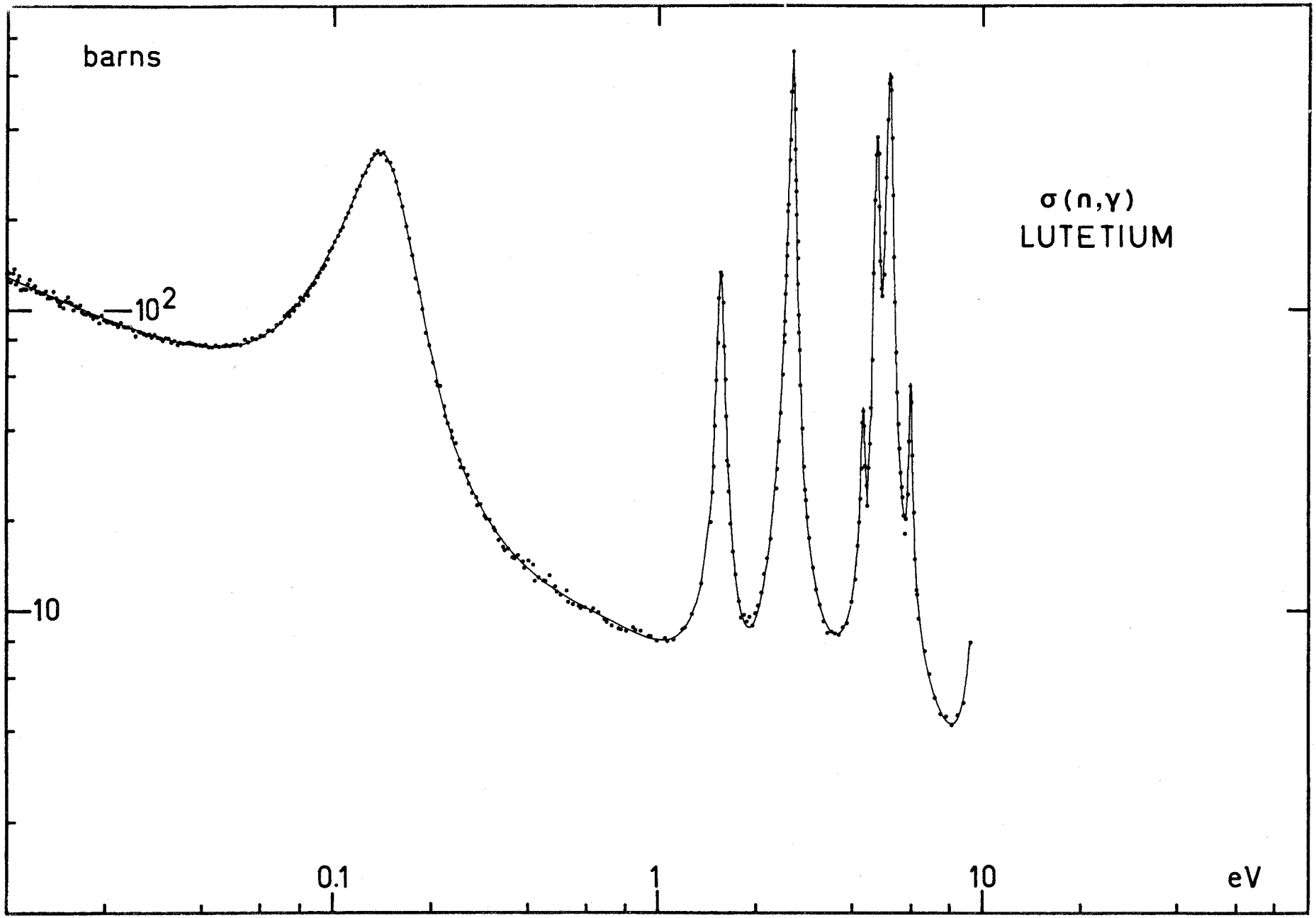
barns
10^2
10
0.1
1
10
eV
σ(n,γ)
LUTETIUM

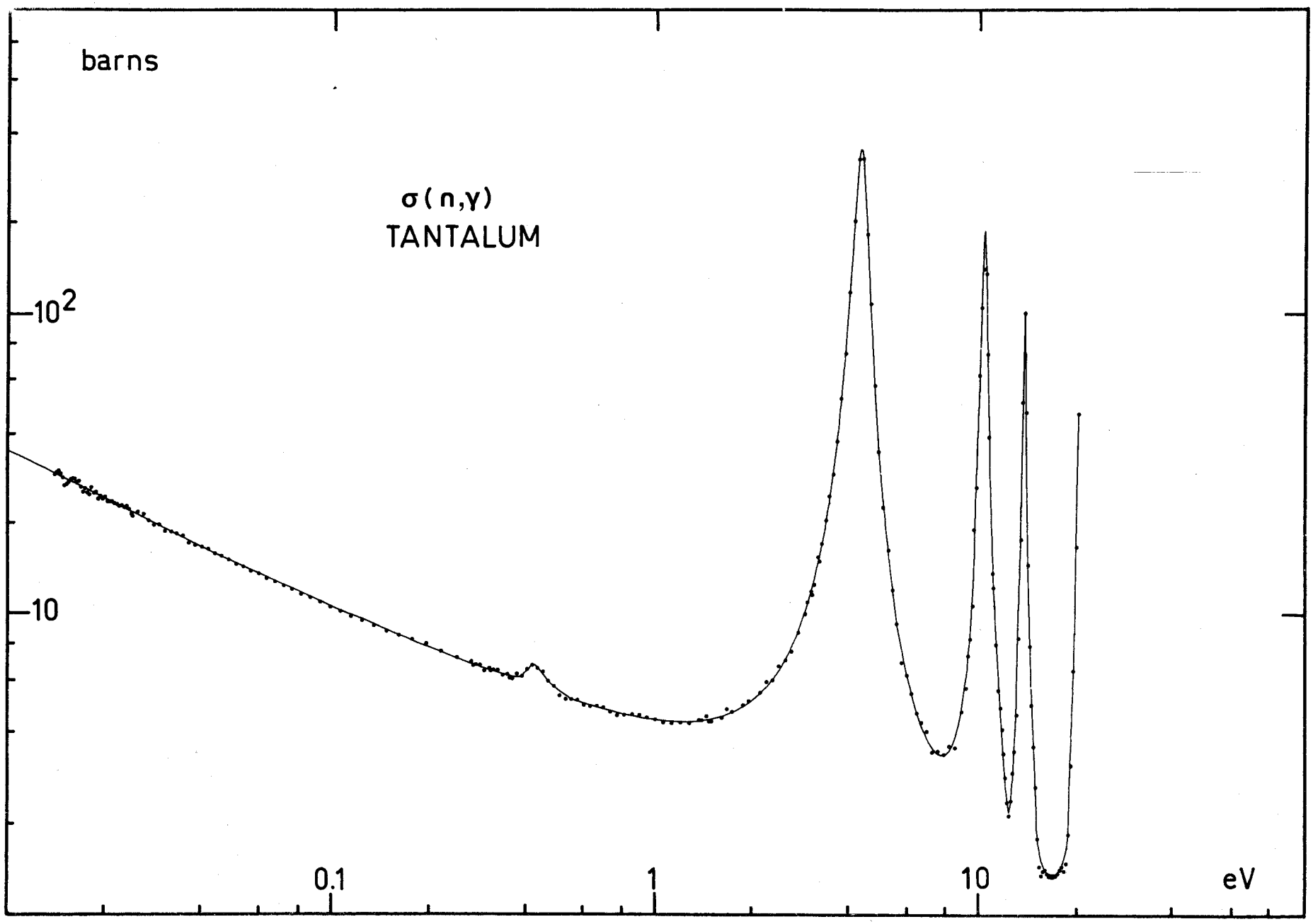
barns
σ(n,γ)
TANTALUM
10²
10
0.1
1
10
eV

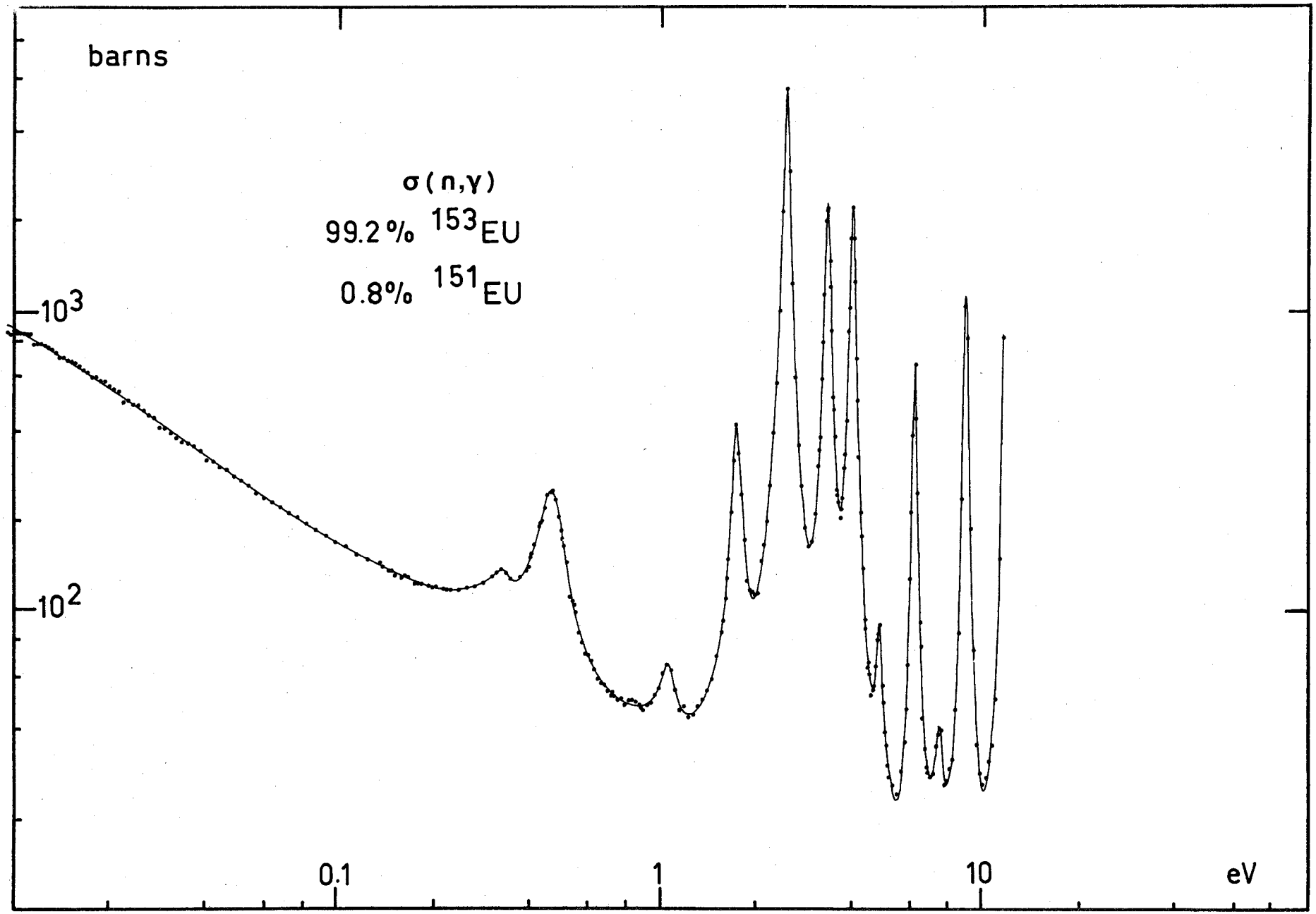
barns
σ(n,γ)
99.2% 153EU
0.8% 151EU
10^3
10^2
0.1
1
10
eV

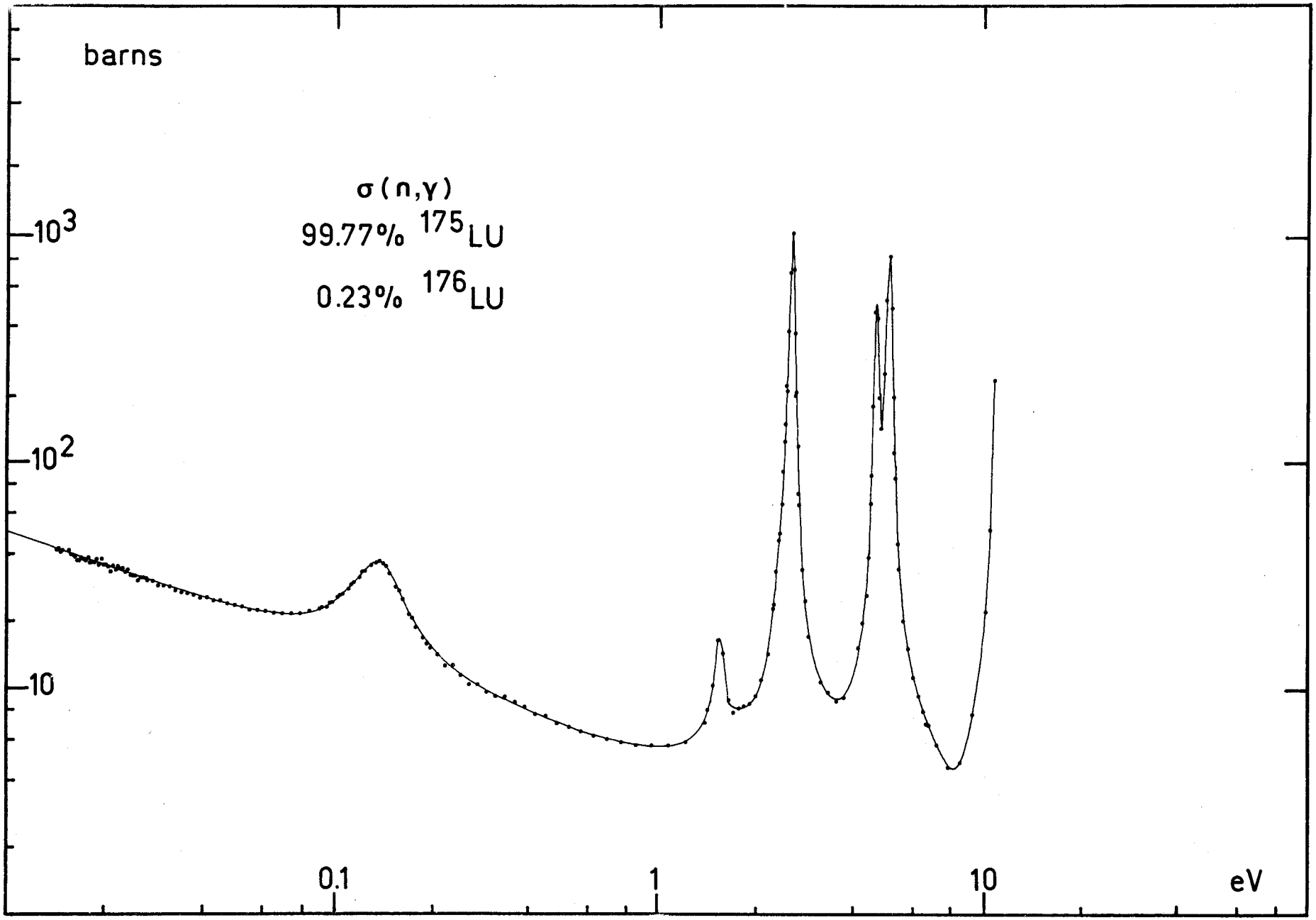
barns
σ(n,γ)
99.77% 175LU
0.23% 176LU
10^3
10^2
10
0.1
1
10
eV

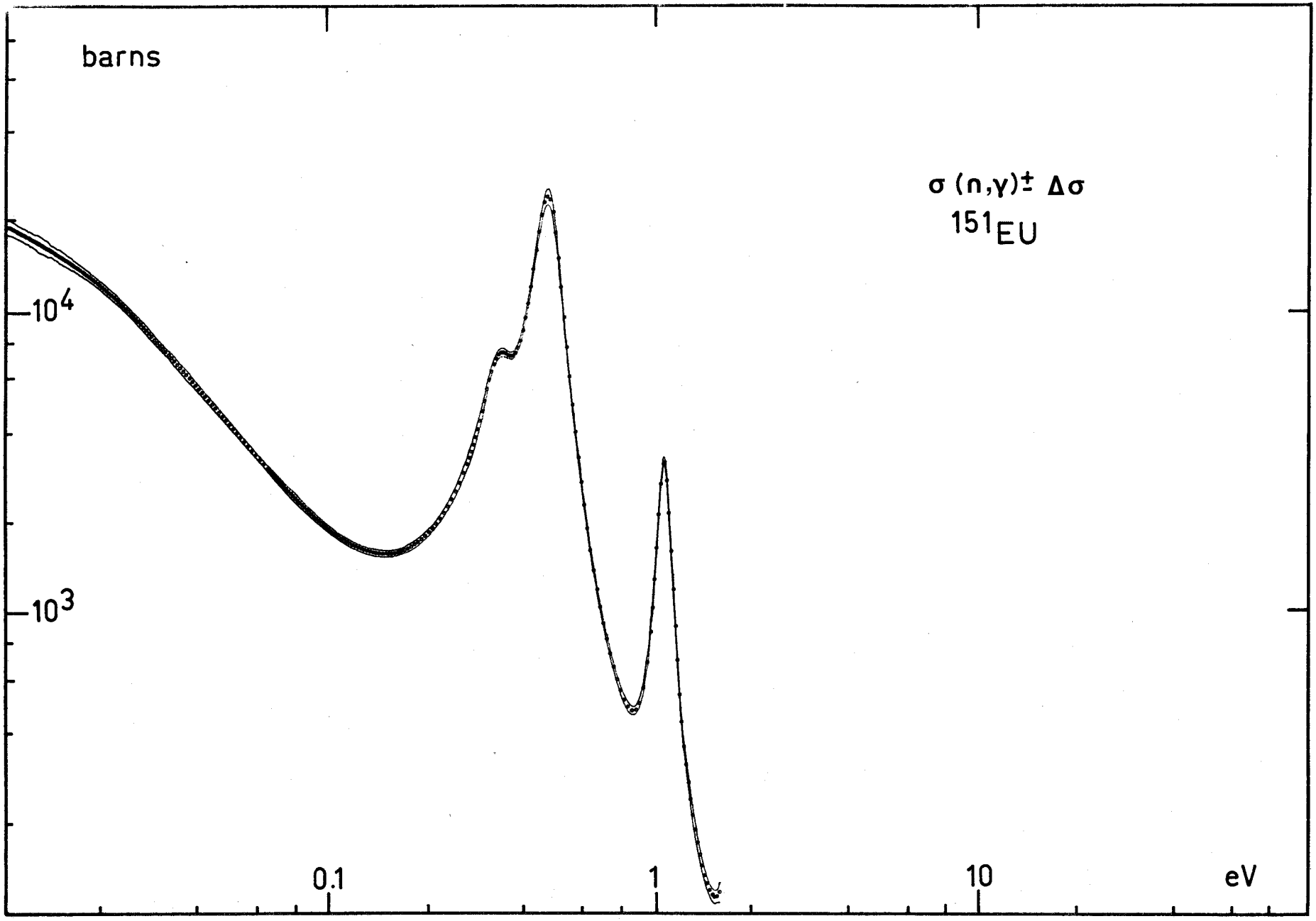
barns
σ (n,γ)± Δσ
151EU
10^4
10^3
0.1
1
10
eV

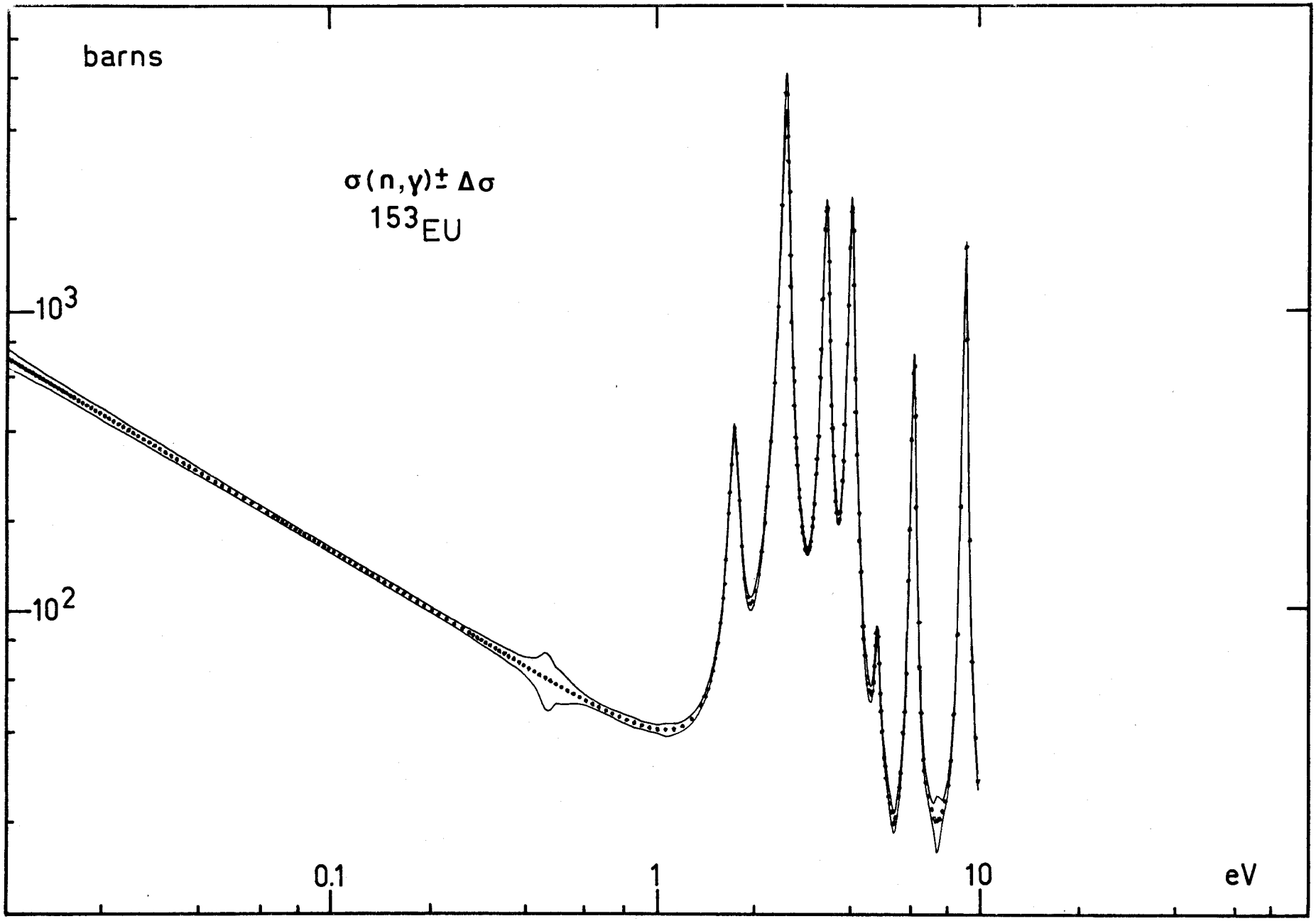
barns
σ(n,γ)± Δσ
153EU
10^3
10^2
0.1
1
10
eV

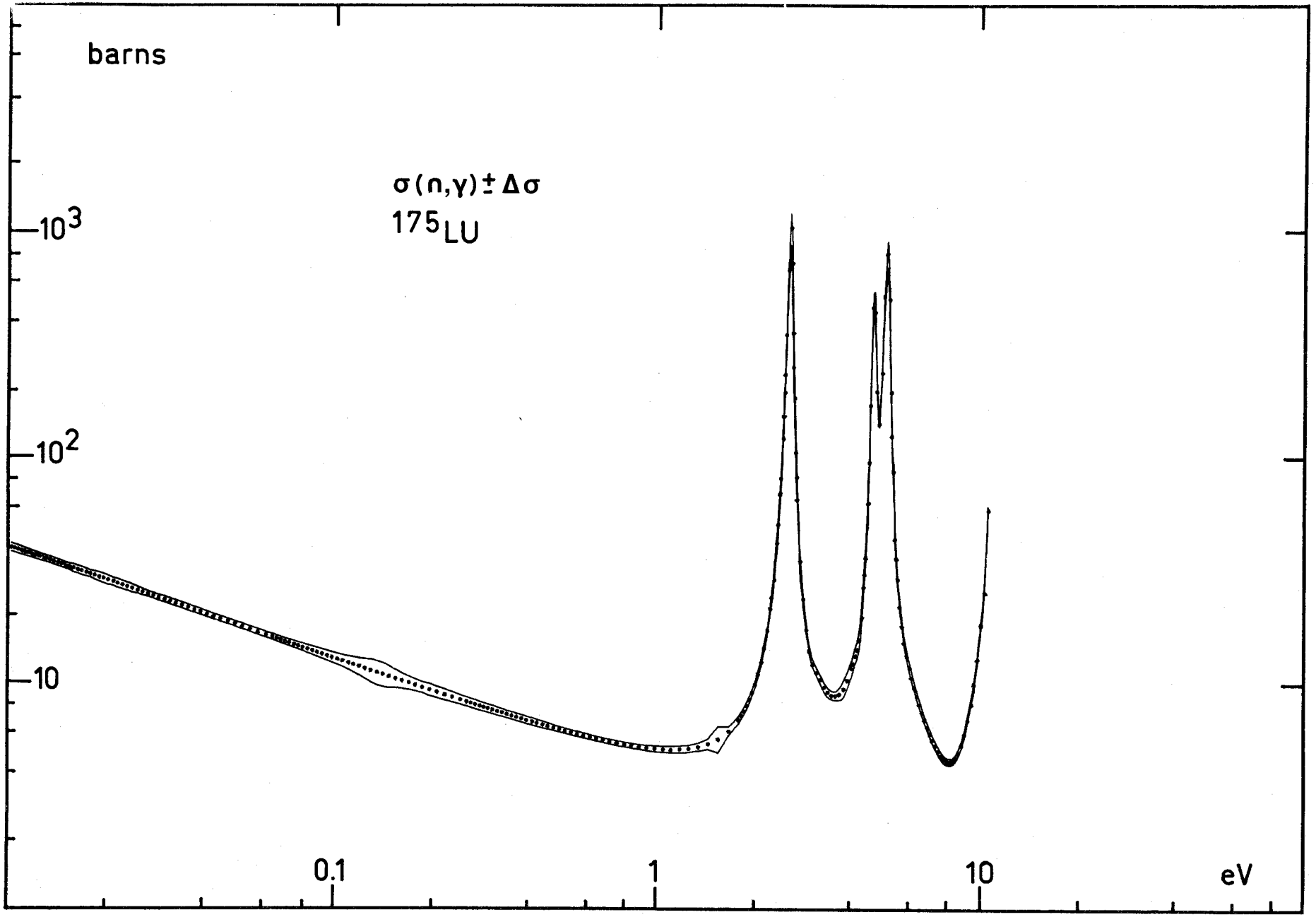
barns
σ(n,γ) ± Δσ
175LU
10^3
10^2
10
0.1
1
10
eV

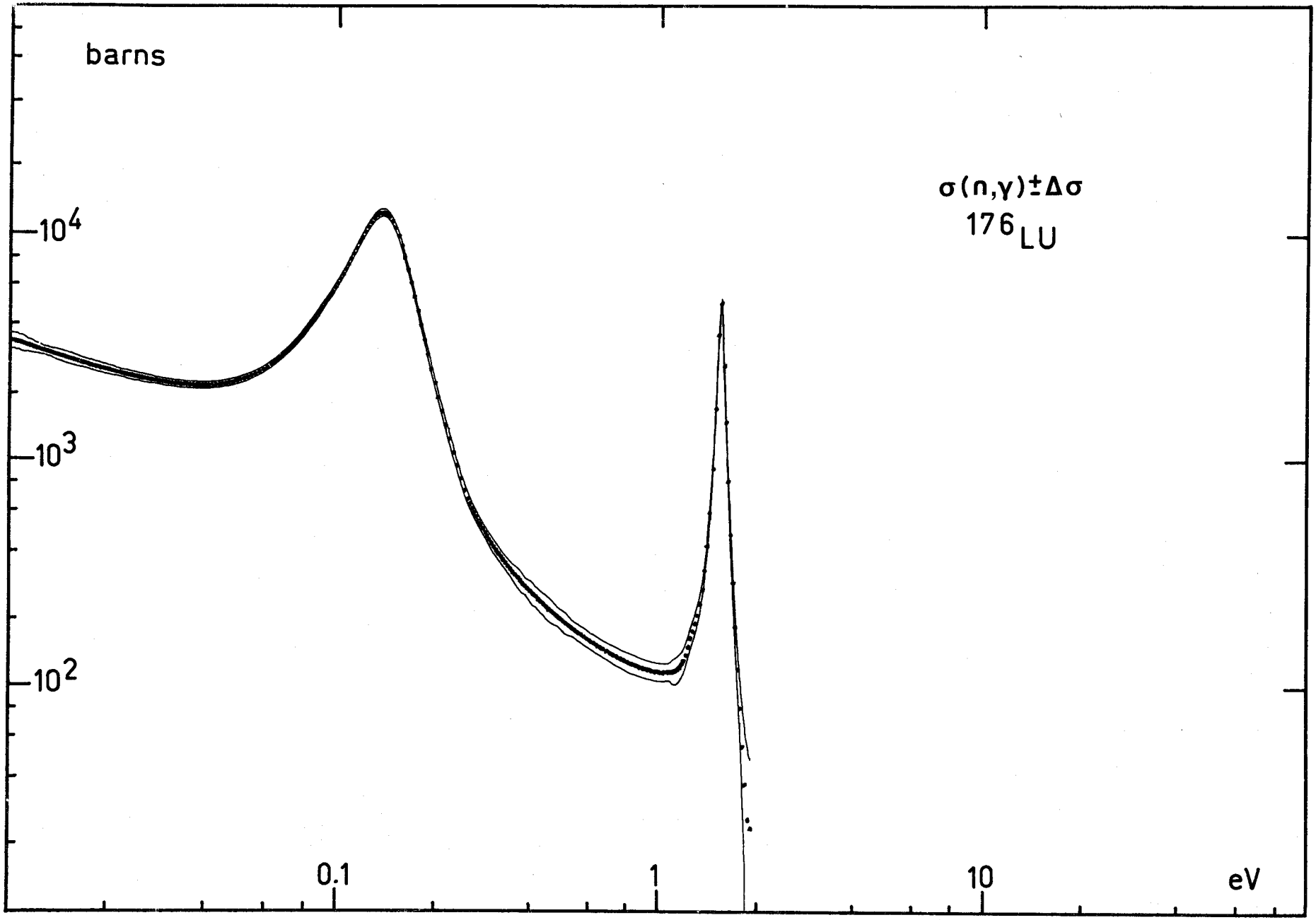
barns
σ(n,γ)±Δσ
176LU
10^4
10^3
10^2
0.1
1
10
eV